arXiv:astro-ph/9602070v1 14 Feb 1996

FERMILAB-Pub-96/023-A

Loop Corrections in Non-Linear Cosmological Perturbation Theory II. Two-point Statistics and Self-Similarity

Román Scoccimarro[1,2] and Joshua A. Frieman[2,3]

[1]Department of Physics and Enrico Fermi Institute, University of Chicago, Chicago, IL 60637

[2]NASA/Fermilab Astrophysics Center, Fermi National Accelerator Laboratory, P.O.Box 500, Batavia, IL 60510

ABSTRACT

We calculate the lowest-order non-linear contributions to the power spectrum, two-point correlation function, and smoothed variance of the density field, for Gaussian initial conditions and scale-free initial power spectra, $P(k) \sim k^n$. These results extend and in some cases correct previous work in the literature on cosmological perturbation theory. Comparing with the scaling behavior observed in N-body simulations, we find that the validity of non-linear perturbation theory depends strongly on the spectral index n. For $n < -1$, we find excellent agreement over scales where the variance $\sigma^2(R) \lesssim 10$; however, for $n \geq -1$, perturbation theory predicts deviations from self-similar scaling (which increase with n) not seen in numerical simulations. This anomalous scaling suggests that the principal assumption underlying cosmological perturbation theory, that large-scale fields can be described perturbatively even when fluctuations are highly non-linear on small scales, breaks down beyond leading order for spectral indices $n \geq -1$. For $n < -1$, the power spectrum, variance, and correlation function in the scaling regime can be calculated using dimensional regularization.

Subject headings: cosmology: large-scale structure of the universe

---

[3]Also Department of Astronomy and Astrophysics, University of Chicago, Chicago, IL 60637

1. Introduction

Several independent arguments suggest that the growth of cosmological density perturbations on large scales can be described by perturbation theory, even when the density and velocity fields are highly non-linear on small scales. For example, analytic and numerical work showed that linear perturbation theory describes the evolution of the large-scale density power spectrum $P(k)$, provided the initial spectrum falls off less steeply than k^4 for small k (Zel'dovich 1965, Peebles 1974, Peebles & Groth 1976, Peebles 1980). In addition, for Gaussian initial conditions, leading-order non-linear perturbative calculations of higher order moments of the density field, e.g., the skewness and kurtosis, agree well with N-body simulations in the weakly non-linear regime, where the variance of the smoothed density field $\sigma^2(R) \equiv \langle \delta^2(R) \rangle \lesssim 0.5 - 1$ (Juszkiewicz, Bouchet & Colombi 1993, Bernardeau 1994, Gaztañaga & Baugh 1995, Baugh, Gaztañaga & Efstathiou 1995). Thus, leading-order perturbation theory has been shown to work surprisingly well in the cases where comparisons with numerical simulations have been made.

The success of leading-order cosmological perturbation theory raises questions: since the perturbation series is most likely asymptotic, what happens beyond leading order—does the agreement with simulations improve or deteriorate? More generally, what sets the limits of perturbation theory, beyond which it breaks down? These questions have become more urgent since it has been shown that leading-order perturbation theory appears to provide an adequate description even on scales where *next-to-leading order* and higher order perturbative contributions would be expected to become important.

To address these questions, one must calculate loop corrections, *i.e.*, corrections *beyond* leading order, in non-linear cosmological perturbation theory (NLCPT). This is the second paper of a series devoted to this topic. In the first paper (Scoccimarro & Frieman 1996), we applied diagrammatic techniques to calculate loop corrections to 1-point cumulants of unsmoothed fields, such as the variance and skewness, for Gaussian initial conditions. Here, we calculate the 1-loop (first non-linear) corrections to the power spectrum, the volume-averaged two-point correlation function, and the variance of the smoothed density field for scale-free initial spectra, $P(k) \sim k^n$. While the linear power spectrum for the Universe is not scale-free (on both observational and theoretical grounds), scale-free spectra are useful approximations over limited ranges of wavenumber k; they also have the advantage of yielding analytic closed form results. In a forthcoming paper, we will present 1-loop corrections to the bispectrum (the three-point cumulant in Fourier space) and the skewness of the smoothed density field for scale-free and cold dark matter spectra.

One-loop corrections to the two-point correlation function and power spectrum have been previously studied in the literature (Juszkiewicz 1981, Vishniac 1983, Juszkiewicz,

Sonoda & Barrow 1984, Coles 1990, Suto & Sasaki 1991, Makino, Sasaki & Suto 1992, Jain & Bertschinger 1994, Baugh & Efstathiou 1994). Multi-loop corrections to the power spectrum were considered by Fry 1994, including the full contributions up to 2 loops and the most important terms at large k in 3- and 4-loop order. Some of our results overlap in particular with the analytic results for the 1-loop power spectrum reported by Suto & Sasaki (1991) and in Makino et al. (1992). However, since we found that some of their expressions contain errors, we present complete corrected expressions for the 1-loop power spectrum. One-loop corrections to the variance were studied numerically for Gaussian smoothing by Łokas et al. (1995). We correct some numerical errors in their results, extend them to include top-hat smoothing and to the average two-point correlation function, and provide analytic derivation of some of the numerical results.

The limiting behavior of the 1-loop corrections on large scales leads us to reconsider the issue of self-similarity in perturbation theory (Davis & Peebles 1977, Peebles 1980). It is commonly accepted that the evolution of density perturbations from scale-free initial conditions in an Einstein-de Sitter universe is statistically self-similar. N-body simulations have generally found self-similar scaling for $-3 < n < 1$, although the results for $n < -1$ have been somewhat ambiguous due to problems of dynamic range in the simulations (Efstathiou et al. 1988, Bertschinger & Gelb 1991, Ryden & Gramann 1991, Gramann 1992, Colombi et al. 1995, Jain 1995, Padmanabhan et al. 1995). The issue of self-similarity in NLCPT has recently been investigated by Jain & Bertschinger (1995), who present arguments that the perturbative evolution is also self-similar. While we do not disagree with their calculations, we start from a different premise regarding cutoffs in the initial spectrum, which leads us to conclude that loop corrections break self-similar scaling if the spectral index $n \geq -1$. In the regime where we do find scaling, $n < -1$, we use dimensional regularization to calculate analytically the asymptotic behavior of the 1-loop power spectrum, variance, and average correlation function; these results agree quite well with the 'universal scaling' extracted from numerical simulations (Hamilton et al. 1991, Peacock & Dodds 1994, Jain, Mo & White 1995).

The paper is organized as follows. In Sec. 2 we discuss non-linear perturbation theory and review the diagrammatic approach developed in (Fry 1984, Goroff et al. 1986, Scoccimarro & Frieman 1996) to the calculation of statistical quantities. Section 3 presents the results of 1-loop calculations for the power spectrum, the smoothed variance, and average two-point correlation function. Self-similarity in perturbation theory is the subject of Sec. 4. We discuss the conditions under which 1-loop corrections exhibit self-similarity and compare our results with the universal scaling hypothesis, based on numerical simulations. Section 5 contains our conclusions.

2. Dynamics and Statistics

2.1. The Equations of Motion

Assuming the universe is dominated by pressureless dust (e.g., cold dark matter), in the single-stream approximation (prior to orbit crossing) one can adopt a fluid description of the cosmological N-body problem. In this limit, the relevant equations of motion correspond to conservation of mass and momentum and the Poisson equation (e.g., Peebles 1980, Scoccimarro & Frieman 1996),

$$\frac{\partial \delta(\mathbf{x},\tau)}{\partial \tau} + \nabla \cdot \{[1+\delta(\mathbf{x},\tau)]\mathbf{v}(\mathbf{x},\tau)\} = 0, \tag{2-1a}$$

$$\frac{\partial \mathbf{v}(\mathbf{x},\tau)}{\partial \tau} + \mathcal{H}(\tau)\ \mathbf{v}(\mathbf{x},\tau) + [\mathbf{v}(\mathbf{x},\tau)\cdot\nabla]\mathbf{v}(\mathbf{x},\tau) = -\nabla\Phi(\mathbf{x},\tau), \tag{2-1b}$$

$$\nabla^2\Phi(\mathbf{x},\tau) = \frac{3}{2}\Omega\mathcal{H}^2(\tau)\delta(\mathbf{x},\tau) \tag{2-1c}$$

Here the density contrast $\delta(\mathbf{x},\tau) \equiv \rho(\mathbf{x},\tau)/\bar{\rho} - 1$, with $\bar{\rho}(\tau)$ the mean density of matter, $\mathbf{v} \equiv d\mathbf{x}/d\tau$ represents the velocity field fluctuations about the Hubble flow, $\mathcal{H} \equiv d\ln a/d\tau$ is the conformal expansion rate, $a(\tau)$ is the cosmic scale factor, $\mathbf{x}$ denote comoving coordinates, $\tau = \int dt/a$ is the conformal time, Φ is the gravitational potential due to the density fluctuations, and the density parameter $\Omega = \bar{\rho}/\rho_c = 8\pi G\bar{\rho}a^2/3\mathcal{H}^2$. Note that we have implicitly assumed the Newtonian approximation to General Relativity, valid on scales less than the Hubble length $a\mathcal{H}^{-1}$. We take the velocity field to be irrotational, so it can be completely described by its divergence $\theta \equiv \nabla\cdot\mathbf{v}$. Equations (2-1) hold in an arbitrary homogeneous and isotropic background Universe which evolves according to the Friedmann equations; henceforth, for simplicity we assume an Einstein-de Sitter background, $\Omega = 1$ (with vanishing cosmological constant), for which $a \propto \tau^2$ and $3\Omega\mathcal{H}^2/2 = 6/\tau^2$.

We take the divergence of Equation (2-1b) and Fourier transform the resulting equations of motion according to the convention

$$\tilde{A}(\mathbf{k},\tau) = \int \frac{d^3x}{(2\pi)^3}\exp(-i\mathbf{k}\cdot\mathbf{x})\ A(\mathbf{x},\tau), \tag{2-2}$$

for the Fourier transform of any field $A(\mathbf{x},\tau)$, where, here and throughout, $\mathbf{k}$ is a comoving wavenumber. This yields

$$\frac{\partial\tilde{\delta}(\mathbf{k},\tau)}{\partial\tau} + \tilde{\theta}(\mathbf{k},\tau) = -\int d^3k_1 \int d^3k_2 \delta_D(\mathbf{k}-\mathbf{k}_1-\mathbf{k}_2)\alpha(\mathbf{k},\mathbf{k}_1)\tilde{\theta}(\mathbf{k}_1,\tau)\tilde{\delta}(\mathbf{k}_2,\tau), \qquad \text{(2-3a)}$$

$$\begin{aligned}\frac{\partial\tilde{\theta}(\mathbf{k},\tau)}{\partial\tau} &+ \mathcal{H}(\tau)\ \tilde{\theta}(\mathbf{k},\tau) + \frac{3}{2}\mathcal{H}^2(\tau)\tilde{\delta}(\mathbf{k},\tau) = \\ &- \int d^3k_1 \int d^3k_2 \delta_D(\mathbf{k}-\mathbf{k}_1-\mathbf{k}_2)\beta(\mathbf{k},\mathbf{k}_1,\mathbf{k}_2)\tilde{\theta}(\mathbf{k}_1,\tau)\tilde{\theta}(\mathbf{k}_2,\tau), \qquad \text{(2-3b)}\end{aligned}$$

(δ_D denotes the three-dimensional Dirac delta distribution), where the functions

$$\alpha(\mathbf{k},\mathbf{k}_1) \equiv \frac{\mathbf{k}\cdot\mathbf{k}_1}{k_1^2}, \qquad \beta(\mathbf{k},\mathbf{k}_1,\mathbf{k}_2) \equiv \frac{k^2(\mathbf{k}_1\cdot\mathbf{k}_2)}{2k_1^2k_2^2} \qquad \text{(2-4)}$$

encode the non-linearity of the evolution (mode coupling) and come from the non-linear terms in the continuity equation (2-1a) and the Euler equation (2-1b) respectively.

2.2. Perturbation Theory Solutions

Equations (2-3) are very difficult to solve in general, being coupled integro-differential equations with no small parameter. The perturbative approach to the problem is to consider perturbations about the linear solution, effectively treating the variance of the linear fluctuations as a small parameter. In this case, Eqs. (2-3) can be formally solved via a perturbative expansion,

$$\tilde{\delta}(\mathbf{k},\tau) = \sum_{n=1}^{\infty} a^n(\tau)\delta_n(\mathbf{k}), \qquad \tilde{\theta}(\mathbf{k},\tau) = \mathcal{H}(\tau)\sum_{n=1}^{\infty} a^n(\tau)\theta_n(\mathbf{k}), \qquad \text{(2-5)}$$

where only the fastest growing mode is taken into account. At small a, the series are dominated by their first terms, and since $\theta_1(\mathbf{k}) = -\delta_1(\mathbf{k})$ from the continuity equation, $\delta_1(\mathbf{k})$ completely characterizes the linear fluctuations. The equations of motion (2-3) determine $\delta_n(\mathbf{k})$ and $\theta_n(\mathbf{k})$ in terms of the linear fluctuations,

$$\delta_n(\mathbf{k}) = \int d^3q_1 \ldots \int d^3q_n \delta_D(\mathbf{k}-\mathbf{q}_1-\ldots-\mathbf{q}_n)F_n^{(s)}(\mathbf{q}_1,\ldots,\mathbf{q}_n)\delta_1(\mathbf{q}_1)\ldots\delta_1(\mathbf{q}_n), \qquad \text{(2-6a)}$$

$$\theta_n(\mathbf{k}) = -\int d^3q_1 \ldots \int d^3q_n \delta_D(\mathbf{k}-\mathbf{q}_1-\ldots-\mathbf{q}_n)G_n^{(s)}(\mathbf{q}_1,\ldots,\mathbf{q}_n)\delta_1(\mathbf{q}_1)\ldots\delta_1(\mathbf{q}_n), \qquad \text{(2-6b)}$$

where $F_n^{(s)}$ and $G_n^{(s)}$ are symmetric homogeneous functions of the wave vectors $\{\,\mathbf{q}_1,\ldots,\mathbf{q}_n\}$ with degree zero. They are constructed from the fundamental mode coupling functions $\alpha(\mathbf{k},\mathbf{k}_1)$ and $\beta(\mathbf{k},\mathbf{k}_1,\mathbf{k}_2)$ according to the recursion relations ($n \geq 2$, see Goroff et al. (1986), Jain & Bertschinger (1994), for a derivation):

$$\begin{aligned} F_n(\mathbf{q}_1,\ldots,\mathbf{q}_n) &= \sum_{m=1}^{n-1} \frac{G_m(\mathbf{q}_1,\ldots,\mathbf{q}_m)}{(2n+3)(n-1)}\Big[(2n+1)\alpha(\mathbf{k},\mathbf{k}_1)F_{n-m}(\mathbf{q}_{m+1},\ldots,\mathbf{q}_n) \\ &+ 2\beta(\mathbf{k},\mathbf{k}_1,\mathbf{k}_2)G_{n-m}(\mathbf{q}_{m+1},\ldots,\mathbf{q}_n)\Big], \end{aligned} \tag{2-7a}$$

$$\begin{aligned} G_n(\mathbf{q}_1,\ldots,\mathbf{q}_n) &= \sum_{m=1}^{n-1} \frac{G_m(\mathbf{q}_1,\ldots,\mathbf{q}_m)}{(2n+3)(n-1)}\Big[3\alpha(\mathbf{k},\mathbf{k}_1)F_{n-m}(\mathbf{q}_{m+1},\ldots,\mathbf{q}_n) \\ &+ 2n\beta(\mathbf{k},\mathbf{k}_1,\mathbf{k}_2)G_{n-m}(\mathbf{q}_{m+1},\ldots,\mathbf{q}_n)\Big], \end{aligned} \tag{2-7b}$$

(where $\mathbf{k}_1 \equiv \mathbf{q}_1 + \ldots + \mathbf{q}_m$, $\mathbf{k}_2 \equiv \mathbf{q}_{m+1} + \ldots + \mathbf{q}_n$, $\mathbf{k} \equiv \mathbf{k}_1 + \mathbf{k}_2$, and $F_1 = G_1 \equiv 1$) and the symmetrization procedure:

$$F_n^{(s)}(\mathbf{q}_1,\ldots,\mathbf{q}_n) = \frac{1}{n!}\sum_{\pi} F_n(\mathbf{q}_{\pi(1)},\ldots,\mathbf{q}_{\pi(n)}), \tag{2-8a}$$

$$G_n^{(s)}(\mathbf{q}_1,\ldots,\mathbf{q}_n) = \frac{1}{n!}\sum_{\pi} G_n(\mathbf{q}_{\pi(1)},\ldots,\mathbf{q}_{\pi(n)}), \tag{2-8b}$$

where the sum is taken over all the permutations π of the set $\{1,\ldots,n\}$. For example, for $n = 2$ we have:

$$F_2^{(s)}(\mathbf{q}_1,\mathbf{q}_2) = \frac{5}{7} + \frac{1}{2}\frac{\mathbf{q}_1\cdot\mathbf{q}_2}{q_1 q_2}\left(\frac{q_1}{q_2}+\frac{q_2}{q_1}\right) + \frac{2}{7}\frac{(\mathbf{q}_1\cdot\mathbf{q}_2)^2}{q_1^2 q_2^2}, \tag{2-9a}$$

$$G_2^{(s)}(\mathbf{q}_1,\mathbf{q}_2) = \frac{3}{7} + \frac{1}{2}\frac{\mathbf{q}_1\cdot\mathbf{q}_2}{q_1 q_2}\left(\frac{q_1}{q_2}+\frac{q_2}{q_1}\right) + \frac{4}{7}\frac{(\mathbf{q}_1\cdot\mathbf{q}_2)^2}{q_1^2 q_2^2}. \tag{2-9b}$$

The perturbation theory kernels have the following properties (Goroff et al. 1986, Wise 1988):

1. As $\mathbf{k} = \mathbf{q}_1 + \ldots + \mathbf{q}_n$ goes to zero, but the individual $\mathbf{q}_i$ do not, $F_n^{(s)} \propto k^2$. This is a consequence of momentum conservation in center of mass coordinates.

2. As some of the arguments of $F_n^{(s)}$ or $G_n^{(s)}$ get large but the total sum $\mathbf{k} = \mathbf{q}_1 + \ldots + \mathbf{q}_n$ stays fixed, the kernels vanish in inverse square law. That is, for $p \gg q_i$, we have:

$$F_n^{(s)}(\mathbf{q}_1, \ldots, \mathbf{q}_{n-2}, \mathbf{p}, -\mathbf{p}) \approx G_n^{(s)}(\mathbf{q}_1, \ldots, \mathbf{q}_{n-2}, \mathbf{p}, -\mathbf{p}) \propto k^2/p^2. \tag{2-10}$$

3. If one of the arguments $\mathbf{q}_i$ of $F_n^{(s)}$ or $G_n^{(s)}$ goes to zero, there is an infrared divergence of the form $\mathbf{q}_i/q_i^2$. This comes from the infrared behavior of the mode coupling functions $\alpha(\mathbf{k}, \mathbf{k}_1)$ and $\beta(\mathbf{k}, \mathbf{k}_1, \mathbf{k}_2)$. There are no infrared divergences as partial sums of several wavevectors go to zero.

2.3. Diagrammatic Expansion of Statistical Quantities

In this work we focus on the non-linear evolution of two-point cumulants of the density field, such as the power spectrum and the volume-average two-point correlation function, and their 1-point counterpart, the variance. These are defined respectively by:

$$\left\langle \tilde{\delta}(\mathbf{k}, \tau) \tilde{\delta}(\mathbf{k}', \tau) \right\rangle_c = \delta_D(\mathbf{k} + \mathbf{k}') P(k, \tau), \tag{2-11}$$

$$\bar{\xi}(R, \tau) \equiv \int \xi(x, \tau) \bar{W}(x) d^3x = \int P(k, \tau) W(kR) d^3k, \tag{2-12}$$

$$\sigma^2(R, \tau) = \int P(k, \tau)\ W^2(kR)\ d^3k. \tag{2-13}$$

Here $\xi(x, \tau) = \int P(k, \tau)\ \exp(i\mathbf{k} \cdot \mathbf{x})\ d^3k$ is the two-point correlation function, and $\bar{W}(x)$ is a window function, with Fourier transform $W(kR)$ which we take to be either a top-hat (TH) or a Gaussian (G),

$$W_{\rm TH}(u) = \frac{3}{u^3}\Big[\sin(u) - u\cos(u)\Big], \tag{2-14}$$

$$W_{\rm G}(u) = \exp(-u^2/2). \tag{2-15}$$

We are interested in calculating the non-linear evolution of these statistical quantities from Gaussian initial conditions in the weakly non-linear regime, $\sigma(R) \lesssim 1$. A systematic

framework for calculating correlations of cosmological fields in perturbation theory has been formulated using diagrammatic techniques (Goroff et al. 1986, Wise 1988, Scoccimarro & Frieman 1996). In this approach, contributions to p-point cumulants of the density field come from connected diagrams with p external (solid) lines and $r = p - 1, p, \ldots$ internal (dashed) lines. The perturbation expansion leads to a collection of diagrams at each order, the leading order being tree-diagrams, the next to leading order 1-loop diagrams and so on. In each diagram, external lines represent the spectral components of the fields we are interested in (e.g., $\delta(\mathbf{k}, \tau)$). Each internal line is labeled by a wave-vector that is integrated over, and represents a linear power spectrum $P_{11}(q, \tau)$. Vertices of order n (i.e., where n internal lines join) represent a $n^{\rm th}$ order perturbative solution δ_n, and momentum conservation is imposed at each vertex. Figure 1 shows the factors associated with vertices and internal lines. To find the contribution of order $2r$ to the *p-point spectrum* of the density field proceed as follows (Scoccimarro & Frieman 1996):

- Draw all distinct connected diagrams containing p vertices (with external lines labeled by $\mathbf{k}_1 \ldots \mathbf{k}_p$) joined by r internal lines. Two diagrams are distinct if they cannot be deformed into each other by moving the vertices and lines without cutting any internal lines (sliding lines over other lines is allowed in the rearrangement process). For each of these diagrams:

  1. Assign a factor of $\delta_D(\mathbf{k}_i - \mathbf{q}_1 - \ldots - \mathbf{q}_n) F_n^{(s)}(\mathbf{q}_1, \ldots, \mathbf{q}_n)$ to each vertex of order n and external momentum $\mathbf{k}_i$ $(i = 1, \ldots, p)$. For the arguments of $F_n^{(s)}$, we use the convention of assigning a positive sign to wave-vectors outgoing from the vertex.
  2. Assign a factor of $P_{11}(q_j, \tau)$ to each internal line labeled by $\mathbf{q}_j$.
  3. Integrate over all $\mathbf{q}_j$ $(j = 1, \ldots, r)$.
  4. Multiply by the symmetry factor of the graph, which is the number of permutations of linear fluctuations (δ_1's) that leaves the graph invariant.
  5. Sum over distinct labelings of external lines, thus generating $p!/(n_1! \ldots n_{2r-p+1}!)$ diagrams (where n_i denotes the number of vertices of order i).

- Add up the resulting expressions for all these diagrams.

To calculate 1-point cumulants, we have to integrate further over the $\mathbf{k}_i$ $(i = 1, \ldots p)$. These integrations are trivial because of the presence of delta functions given by rule 1, so we are left only with integrations over the $\mathbf{q}_j$'s. Also, since the $p!/(n_1! \ldots n_{2r-p+1}!)$ diagrams generated by rule 5 become equal contributions when the integration over external lines is performed, to find the contribution of order $2r$ to the *p^{th}-order 1-point cumulant* of the density field we replace rule 5 by the following:

- 5a. Integrate over $\mathbf{k}_i$ $(i = 1, \ldots p)$ and multiply by the multinomial weight $p!/(n_1! \ldots n_{2r-p+1}!)$.

Furthermore, when calculating cumulants of the *smoothed* density field, we add a window function at each vertex, giving instead of rule 1 (see Fig. 1):

- 1a. Assign a factor of $\delta_D(\mathbf{k}_i - \mathbf{q}_1 - \ldots - \mathbf{q}_n) F_n^{(s)}(\mathbf{q}_1, \ldots, \mathbf{q}_n) W(k_i R)$ to each vertex of order n and external momentum $\mathbf{k}_i$ $(i = 1, \ldots, p)$.

According to the above diagrammatic rules, we can write the loop expansion for the power spectrum up to one-loop corrections as

$$P(k,\tau) = P^{(0)}(k,\tau) + P^{(1)}(k,\tau) + \ldots, \tag{2-16}$$

where the superscript (n) denotes an n-loop contribution, the tree-level (0-loop) contribution is just the linear spectrum,

$$P^{(0)}(k,\tau) = P_{11}(k,\tau), \tag{2-17}$$

with $a^2(\tau)\langle\delta_1(\mathbf{k})\delta_1(\mathbf{k}')\rangle_c = \delta_D(\mathbf{k}+\mathbf{k}')P_{11}(k,\tau)$, and the 1-loop contribution consists of two terms,

$$P^{(1)}(k,\tau) = P_{22}(k,\tau) + P_{13}(k,\tau), \tag{2-18}$$

with (see Fig. 2):

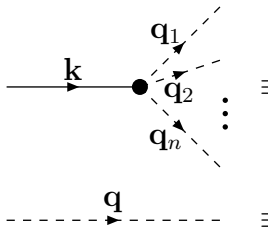

$$\equiv \quad \delta_D(\mathbf{k} - \mathbf{q}_1 - \ldots - \mathbf{q}_n) F_n^{(s)}(\mathbf{q}_1, \ldots, \mathbf{q}_n) W(kR)$$

$$\equiv \quad P_{11}(q,\tau)$$

Fig. 1.— Diagrammatic rules for vertices and internal lines for density field fluctuations smoothed with window W at radius R.

$$P_{22}(k,\tau) \equiv 2\int [F_2^{(s)}(\mathbf{k}-\mathbf{q},\mathbf{q})]^2 P_{11}(|\mathbf{k}-\mathbf{q}|,\tau)P_{11}(q,\tau)d^3q, \tag{2-19a}$$

$$P_{13}(k,\tau) \equiv 6\int F_3^{(s)}(\mathbf{k},\mathbf{q},-\mathbf{q})P_{11}(k,\tau)P_{11}(q,\tau)d^3q. \tag{2-19b}$$

Here P_{ij} denotes the amplitude given by the above rules for a connected diagram representing the contribution from $\langle\delta_i\delta_j\rangle_c$ to the power spectrum. We have assumed Gaussian initial conditions, for which P_{ij} vanishes if $i+j$ is odd.

For the smoothed variance and average two-point correlation function we write

$$\sigma^2(R) = \sigma_\ell^2(R)\Big(1 + s^{(1)}\ \sigma_\ell^2(R) + \dots\Big), \tag{2-20a}$$

$$\bar{\xi}(R) = \bar{\xi}_\ell(R)\Big(1 + x^{(1)}\ \bar{\xi}_\ell(R) + \dots\Big), \tag{2-20b}$$

where $\sigma_\ell^2(R)$ and $\bar{\xi}_\ell(R)$ denote the variance and average two-point correlation function in linear theory (given by (2-13) and (2-12) with $P = P_{11}$); the dimensionless 1-loop amplitudes are

$$s^{(1)}(R) \equiv \frac{1}{\sigma_\ell^4(R)}\int P^{(1)}(k,\tau)\ W^2(kR)\ d^3k, \tag{2-21a}$$

$$x^{(1)}(R) \equiv \frac{1}{\bar{\xi}_\ell^2(R)}\int P^{(1)}(k,\tau)\ W(kR)\ d^3k. \tag{2-21b}$$

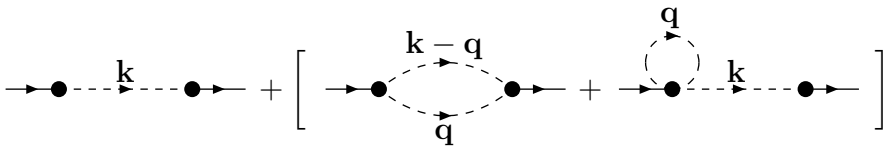

(P_{11}) (P_{22}) (P_{13})

Fig. 2.— Diagrams for the power spectrum up to one loop. See Eqs. (2-19) for diagram amplitudes.

A convenient property of these dimensionless amplitudes is the following: if one defines the correlation length $R_0^{(\ell)}$ in linear theory as the scale where the smoothed linear variance is unity, $\sigma_\ell^2(R_0^{(\ell)}) = 1$, then $s^{(1)}(R_0^{(\ell)}) = \sigma^2(R_0^{(\ell)}) - 1$ is just the non-linear correction to the variance at this scale.

3. Results

3.1. One-Loop Power Spectrum

We consider a linear (tree-level) power spectrum $P_{11}(k,\tau)$ given by a truncated power-law,

$$P_{11}(k,\tau) \equiv \begin{cases} A\ a^2(\tau)\ k^n & \text{if } \epsilon \le k \le k_c, \\ 0 & \text{otherwise,} \end{cases} \tag{3-1}$$

where A is a normalization constant, and the infrared and ultraviolet cutoffs ϵ and k_c are imposed in order to regularize the required radial integrations (Scoccimarro & Frieman 1996). In a cosmological N-body simulation, they would correspond roughly to the inverse comoving box size and lattice spacing (or interparticle separation) respectively. In the absence of the cutoffs, the spectrum (3-1) would be scale-free. We write the one-loop power spectrum contributions as

$$P_{ij}(k,\tau) \equiv \pi A^2 a^4(\tau)\ k_c^{2n+3}\ p_{ij}(n; x, \Lambda), \tag{3-2}$$

where the dimensionless 1-loop spectrum $p^{(1)} = p_{22} + p_{13}$, and we have introduced dimensionless wavenumber variables,

$$x \equiv k/k_c, \qquad \Lambda \equiv k_c/\epsilon. \tag{3-3}$$

From Eq. (2-19a) we obtain (defining $t \equiv q/k_c$):

$$p_{22}(n; x, \Lambda) \equiv \frac{x^4}{49} \int_{1/\Lambda}^{1} dt\ t^n \int_{\lambda_{min}(x,t)}^{\lambda_{max}(x,t,\Lambda)} d\lambda\ (x^2 + t^2 - 2xt\lambda)^{n/2-2}\ (3t - 7x\lambda - 10t\lambda^2)^2, \tag{3-4}$$

when $x \leq 2$; otherwise $p_{22}(n; x, \Lambda) = 0$. The constraint on the angular integration variable $\lambda \equiv (\mathbf{k} \cdot \mathbf{q})/(kq)$ comes from the cutoff dependence of $P_{11}(|\mathbf{k} - \mathbf{q}|, \tau)$, which gives:

$$\lambda_{min}(x, t) \equiv \mathrm{Max}\left\{-1, \frac{x^2 + t^2 - 1}{2xt}\right\}, \tag{3-5a}$$

$$\lambda_{max}(x, t, \Lambda) \equiv \mathrm{Min}\left\{1, \frac{x^2 + t^2 - \Lambda^{-2}}{2xt}\right\}, \tag{3-5b}$$

Care must be taken when dealing with the limits imposed by Eqs. (3-5a) and (3-5b), especially in the cases $n = -1, -2$. On the other hand, integration over angular variables in Eq. (2-19b) is straightforward, and we obtain:

$$\begin{aligned} p_{13}(n; x, \Lambda) \;\equiv\; & x^n \int_{1/\Lambda}^{1} dt\; t^{n+2} \Bigg[\frac{(6x^6 - 79x^4t^2 + 50x^2t^4 - 21t^6)}{63x^2t^4} + \frac{(t^2 - x^2)^3\,(7t^2 + 2x^2)}{42x^3t^5} \\ & \times \ln\frac{|x + t|}{|x - t|} \Bigg], \end{aligned} \tag{3-6}$$

for $\Lambda^{-1} \leq x \leq 1$; otherwise $p_{13}(n; x, \Lambda) = 0$.

In the following subsections we give results for p_{13} and p_{22} in the limit $\Lambda = k_c/\epsilon \to \infty$ up to terms of order Λ^0, for spectral indices $n = 1, 0, -1, -2$. We also give their asymptotic behavior at large scales. From the properties of the perturbation theory kernels given in Sec. 2.2 and Eqs. (2-19), one would naively expect that as $x \to 0$:

$$p_{22}(n; x, \Lambda) \propto x^4 \sim (k/k_c)^4, \qquad p_{13}(n; x, \Lambda) \propto x^{n+2} \sim (k/k_c)^{n+2}. \tag{3-7}$$

Although this is certainly correct for p_{22} when $x \ll \Lambda^{-1}$ (i.e., $k \ll \epsilon$), the expressions below correspond to p_{22} and p_{13} *after* the limit $\Lambda \to \infty$ has been taken and therefore exhibit a different kind of asymptotic behavior (corresponding to $0 \leftarrow \epsilon < k \ll k_c$). This deviation from the expected scaling becomes more pronounced as n decreases, since infrared effects ($\epsilon \to 0$) become more important with the increase of large-scale power. As we will see, Eq. (3-7) is obeyed by p_{22} only when $n \geq 1$ and by p_{13} when $n \geq 0$.

Our results below are equivalent to those of Makino et al. (1992) in the case of p_{13}, but they differ for p_{22} in two respects. First, their expressions for p_{22} are only valid for $x < 1$; they did not seem to consider that p_{22} is non-vanishing up to $x = 2$, and the region

$1 \leq x \leq 2$ requires a separate integration when n is odd. In addition, for n even, their series expansions for the dilogarithms do not converge in this region. The second difference comes from the fact that for $n = -1, -2$, p_{22} develops a divergence at $x = 1$, and the expressions for p_{22} must be modified in a region of radius Λ^{-1} about $x = 1$. This singularity is integrable, giving a finite contribution to the 1-loop correction to the variance. Finally, some of their resulting expressions for $p^{(1)}$ contain typographic errors. We have checked our expressions by analytically integrating them and verifying that they correctly reproduce the unsmoothed 1-loop coefficients $s^{(1)}$ given by Scoccimarro & Frieman (1996). For comparison, we also plot (but do not give explicit expressions for) the 1-loop power spectrum in the Zel'dovich approximation.

3.1.1. $n = 1$

For $n = 1$, the dimensionless 1-loop power spectrum contributions are

$$\begin{aligned} p_{13}(1;x) &= -\frac{1}{21x} + \frac{52x}{315} - \frac{181x^3}{315} - \frac{2x^5}{21} + \ln\left(\frac{1+x}{1-x}\right)\frac{(5 - 19x^2 + 25x^4 - 5x^6 + 10x^8)}{210x^2} \\ &\quad + \frac{8x^5}{105}\ln\left(\frac{1-x^2}{x^2}\right), \end{aligned} \tag{3-8}$$

$$p_{22}(1;x) = \frac{18x^4}{49} - \frac{13x^5}{98} - \frac{20x^6}{1029} + \frac{x^7}{49}, \qquad \text{if } x \leq 1, \tag{3-9}$$

$$p_{22}(1;x) = -\frac{320}{1029x} + \frac{16x}{49} + \frac{2x^3}{3} - \frac{18x^4}{49} - \frac{5x^5}{42} + \frac{20x^6}{1029} + \frac{x^7}{49}, \qquad \text{if } 1 \leq x \leq 2, \tag{3-10}$$

and the 1-loop reduced power spectrum is then (see Fig. 3):

$$\begin{aligned} p^{(1)}(n=1; x = k/k_c \leq 1) &= -\frac{1}{21x} + \frac{52x}{315} - \frac{181x^3}{315} + \frac{18x^4}{49} - \frac{67x^5}{294} - \frac{20x^6}{1029} + \frac{x^7}{49} \\ &\quad + \ln\left(\frac{1+x}{1-x}\right)\frac{(5 - 19x^2 + 25x^4 - 5x^6 + 10x^8)}{210x^2} \\ &\quad + \frac{8x^5}{105}\ln\left(\frac{1-x^2}{x^2}\right), \end{aligned} \tag{3-11}$$

with $p^{(1)}(x) = p_{22}(x)$ when $1 \leq x \leq 2$. For $x \ll 1$ we get:

$$p_{13}(1;x) \approx p^{(1)}(1;x) \approx -\frac{122}{315}x^3 + \mathcal{O}(x^5), \tag{3-12}$$

$$p_{22}(1;x) \approx \frac{18}{49}x^4 + \mathcal{O}(x^5). \tag{3-13}$$

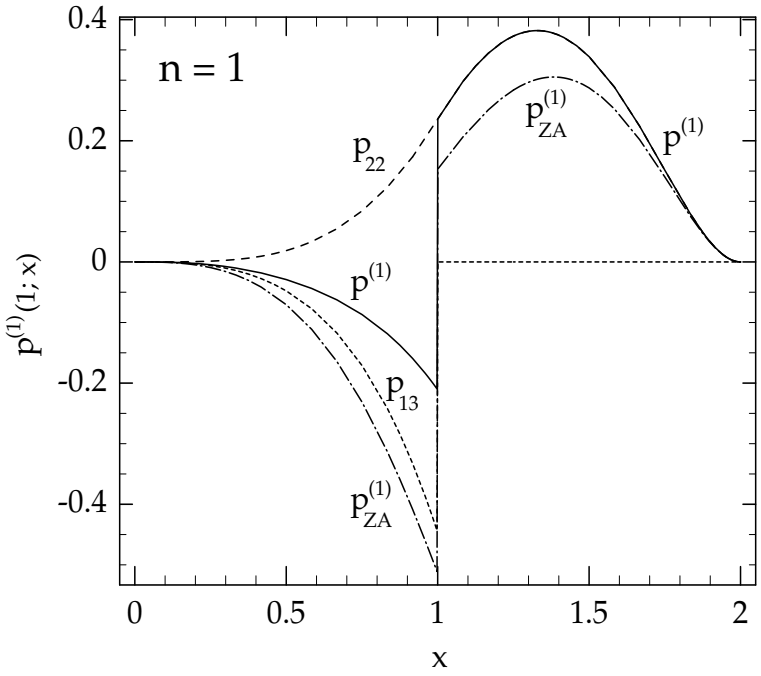

Fig. 3.— One-loop corrections to the power spectrum for $n = 1$. The solid line shows $p^{(1)}(1;x)$ as a function of $x \equiv k/k_c$. Dashed lines correspond to the contribution of individual diagrams, $p_{22}(1;x)$ (long-dashed) and $p_{13}(1;x)$ (short-dashed), whereas the dot-dashed line shows $p^{(1)}(1;x)$ in the Zel'dovich approximation.

3.1.2. $n = 0$

For $n = 0$, the 1-loop power spectrum contributions are

$$p_{13}(0;x) = -\frac{1}{18x^2} + \frac{157}{756} - \frac{269x^2}{252} - \frac{\pi^2 x^3}{84} - \frac{x^4}{21} + \ln\left(\frac{1+x}{1-x}\right) \times\frac{(x^2-1)}{504x^3}(-14 + 43x^2 - 47x^4 + 12x^6) + \frac{x^3}{42}[\mathrm{Li}_2(x) - \mathrm{Li}_2(-x)], \tag{3-14}$$

$$p_{22}(0;x\leq 2) = \frac{25}{98}+\frac{25x}{196}-\frac{10x^2}{147}-\frac{5x^3}{392}+\frac{29\pi^2x^3}{294}+\frac{3x^4}{49}-\frac{65x^5}{1176}+\frac{x^7}{196}+\ln|x-1| \times\frac{(25-15x^2-16x^4+6x^6+29x^4\ln x)}{98x}-\frac{29x^3}{98}\Big[\frac{1}{2}\ln^2(x)+\mathrm{Re}[\mathrm{Li}_2(x)] +\mathrm{Li}_2\left(\frac{x-1}{x}\right)\Big], \quad (3\text{-}15)$$

where Li_2 denotes the dilogarithm, defined by (Lewin 1981)

$$\mathrm{Li}_2(x)\equiv-\int_0^x dz\ \frac{\ln(1-z)}{z}, \quad (3\text{-}16)$$

which has the series expansion for small argument ($x\leq 1$):

$$\mathrm{Li}_2(x)=\sum_{m=1}^{\infty}\frac{x^m}{m^2}. \quad (3\text{-}17)$$

The resulting 1-loop power spectrum is (Fig. 4)

$$p^{(1)}(0;x\leq 1) = -\frac{1}{18x^2}+\frac{2449}{5292}+\frac{25x}{196}-\frac{2003x^2}{1764}-\frac{5x^3}{392}+\frac{17\pi^2x^3}{196}+\frac{2x^4}{147}-\frac{65x^5}{1176}+\frac{x^7}{196} +\ln(1+x)\frac{(x^2-1)}{504x^3}(-14+43x^2-47x^4+12x^6)-\frac{29x^3}{196}\ln^2(x) +\frac{(-98+1299x^2-1170x^4-163x^6+132x^8+1044x^6\ln x)}{3528x^3}\ln(1-x) -\frac{40x^3}{147}\mathrm{Li}_2(x)-\frac{x^3}{42}\mathrm{Li}_2(-x)-\frac{29x^3}{98}\mathrm{Li}_2\left(\frac{x-1}{x}\right), \quad (3\text{-}18)$$

and $p^{(1)}(x)=p_{22}(x)$ when $1\leq x\leq 2$.

For $x\ll 1$ we have:

$$p_{13}(0;x) \approx p^{(1)}(0;x)\approx-\frac{244}{315}x^2+\mathcal{O}(x^3), \quad (3\text{-}19)$$

$$p_{22}(0;x) \approx \frac{29\pi^2}{196}x^3+\mathcal{O}(x^4). \quad (3\text{-}20)$$

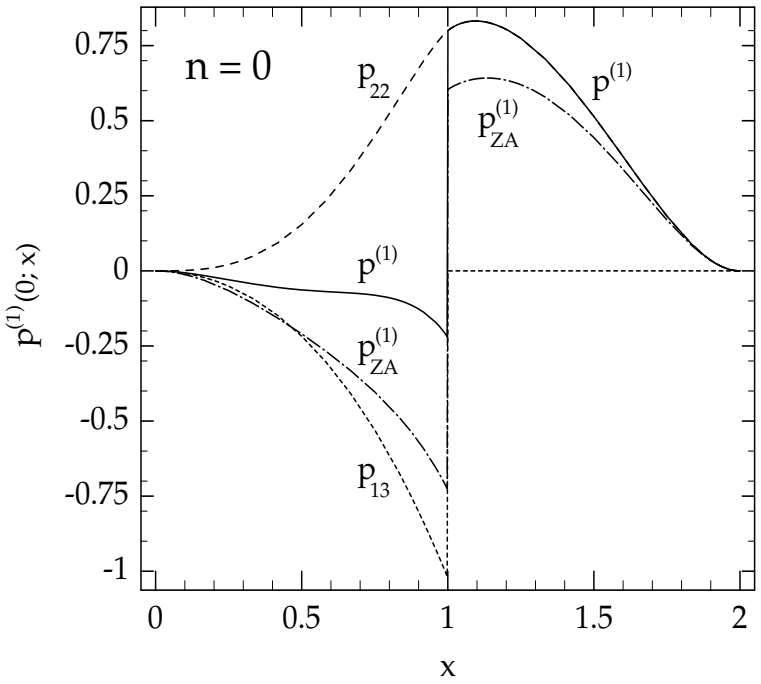

Fig. 4.— Same as Fig. 3 but for $n = 0$.

3.1.3. $n = -1$

For $n \leq -1$, the 1-loop contributions are infrared-divergent and therefore depend on the infrared cutoff through $\Lambda = k_c/\epsilon$,

$$p_{13}(-1;x,\Lambda) = -\frac{4x}{3}\ln\Lambda - \frac{1}{15x^3} + \frac{88}{315x} - \frac{11x}{189} - \frac{2x^3}{63} + \ln\left(\frac{1+x}{1-x}\right) \times\frac{(21-95x^2+225x^4+15x^6+10x^8)}{630x^4} + \frac{88x}{315}\ln\left(\frac{1-x^2}{x^2}\right), \quad (3\text{-}21)$$

$$p_{22}(-1;x,\Lambda) = \frac{4x}{3}\ln\Lambda + \frac{80x}{147} + \frac{2x^2}{3} + \frac{x^3}{3} + \frac{44x^4}{441} + \frac{2x^5}{49} + \frac{x^7}{441} + \frac{2x}{3}\ln[(1-x)x^2], \qquad x \leq 1-\Lambda^{-1}, \quad (3\text{-}22)$$

$$p_{22}(-1;x,\Lambda) = \frac{2x}{3}\ln\Lambda + \frac{160}{147x} + \frac{x^3}{3} + \frac{2x^5}{49} + \frac{x^7}{441} + \frac{2x}{3}\ln(x) - \frac{(x-1)^2}{147x}(50+100x +105x^2+12x^3+6x^4)\,\Lambda - \frac{(x-1)^3}{882x}(15+45x+60x^2+60x^3+12x^4$$

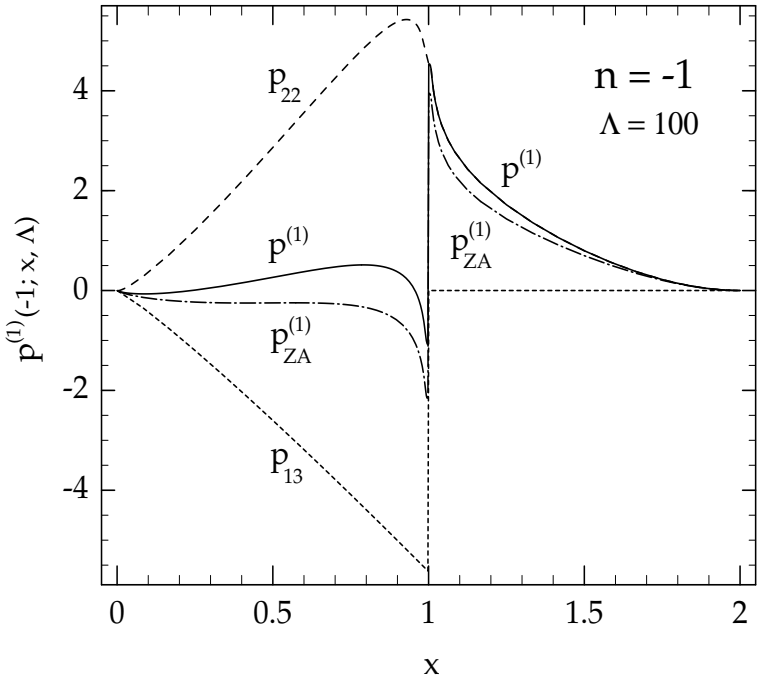

Fig. 5.— Same as Fig. 3 but for $n = -1$ and $\Lambda \equiv k_c/\epsilon = 100$.

$$+4x^5)\Lambda^3, \qquad 1-\Lambda^{-1} \le x \le 1+\Lambda^{-1} \tag{3-23}$$

$$p_{22}(-1;x) = \frac{320}{147x} - \frac{80x}{147} - \frac{2x^2}{3} + \frac{x^3}{3} - \frac{44x^4}{441} + \frac{2x^5}{49} + \frac{x^7}{441} - \frac{2x}{3}\ln(x-1), \qquad 1+\Lambda^{-1} \le x \le 2, \tag{3-24}$$

The 1-loop correction is then

$$\begin{aligned} p^{(1)}(-1;x) &= -\frac{1}{15x^3} + \frac{88}{315x} + \frac{643x}{1323} + \frac{2x^2}{3} + \frac{19x^3}{63} + \frac{44x^4}{441} + \frac{2x^5}{49} + \frac{x^7}{441} \\ &\quad + \frac{(21 - 95x^2 + 225x^4 + 15x^6 + 10x^8)}{630x^4}\ln\left(\frac{1+x}{1-x}\right) + \frac{298x}{315}\ln(1-x) \\ &\quad + \frac{244x}{315}\ln(x) + \frac{88x}{315}\ln(1+x), \qquad x \le 1-\Lambda^{-1}, \end{aligned} \tag{3-25}$$

whereas when $1 \le x \le 2$ we have $p^{(1)}(-1;x) = p_{22}(-1;x)$. For $x \ll 1$ we get:

$$p_{13}(-1;x,\Lambda) \approx -\frac{4x}{3}\ln\Lambda + \frac{128}{225}x - \frac{176x}{315}\ln(x) + \mathcal{O}(x^3), \tag{3-26}$$

$$p_{22}(-1;x,\Lambda) \approx \frac{4x}{3}\ln\Lambda + \frac{80}{147}x + \frac{4x}{3}\ln(x) + \mathcal{O}(x^4), \tag{3-27}$$

$$p^{(1)}(-1;x) \approx \frac{12272}{11025}x + \frac{244x}{315}\ln(x) + \mathcal{O}(x^3). \tag{3-28}$$

In this limit, the divergences cancel; note, however, that the $\Lambda \to \infty$ divergence in p_{22} in the region $1-\Lambda^{-1} \le x \le 1+\Lambda^{-1}$ is uncancelled, although the 'size' of the divergent region shrinks to zero.

3.1.4. $n = -2$

For $n = -2$, the 1-loop terms are

$$\begin{aligned} p_{13}(-2;x,\Lambda) &= -\frac{4}{3}\Lambda - \frac{1}{12x^4} + \frac{107}{252x^2} + \frac{5\pi^2}{28x} + \frac{82}{63} - \frac{x^2}{42} + \ln\left(\frac{1+x}{1-x}\right)\frac{(x^2-1)}{168x^5} \\ &\quad \times(-7+31x^2+4x^4+2x^6) + \frac{5}{14x}[\mathrm{Li}_2(-x) - \mathrm{Li}_2(x)], \end{aligned} \tag{3-29}$$

$$\begin{aligned} p_{22}(-2;x,\Lambda) &= \frac{2}{3}\Lambda + \frac{75}{1568x} + \frac{25\pi^2}{196x} + \frac{15x}{392} + \frac{29x^3}{392} + \frac{3x^5}{196} + \frac{x^7}{784} + \frac{\Lambda^2}{196x}(-50+82x^2 \\ &\quad -29x^4 - 3x^6 - 30x^2\ln x) + \frac{\Lambda^4}{1568x}(25 - 60x^2 + 63x^4 - 24x^6 - 4x^8 \\ &\quad +44x^4\ln x), \qquad 1-\Lambda^{-1} \le x \le 1+\Lambda^{-1} \end{aligned} \tag{3-30}$$

whereas when $x \le 1-\Lambda^{-1}$ or $x \ge 1+\Lambda^{-1}$ we have:

$$\begin{aligned} p_{22}(-2;x,\Lambda) &= \frac{4}{3}\theta(1-x)\Lambda + \frac{1}{2(x-1)} + \frac{25\pi^2}{98x} - \frac{205}{392} - \frac{309x}{784} - \frac{11x^2}{392} + \frac{53x^3}{1568} + \frac{3x^5}{196} \\ &\quad + \frac{x^7}{784} - \frac{75}{196x}\ln^2(x) + \ln|x-1|\frac{(-1001+60x^2-11x^4+300\ln x)}{392x} \\ &\quad - \frac{75}{98x}\left[\mathrm{Re}[\mathrm{Li}_2(x)] + \mathrm{Li}_2\left(\frac{x-1}{x}\right)\right], \end{aligned} \tag{3-31}$$

where $\theta(x)$ is the step function. This gives:

$$
\begin{aligned}
p^{(1)}(-2;x) &= -\frac{1}{12x^4}+\frac{107}{252x^2}+\frac{1}{2(x-1)}+\frac{85\pi^2}{196x}+\frac{2747}{3528}-\frac{309x}{784}-\frac{61x^2}{1176}+\frac{53x^3}{1568}+\frac{3x^5}{196} \\
&+\frac{x^7}{784}-\frac{75}{196x}\ln^2(x)+\ln(1-x)\frac{(-1001+60x^2-11x^4+300\ln x)}{392x} \\
&+\ln\Big(\frac{1+x}{1-x}\Big)\frac{(x^2-1)}{168x^5}(-7+31x^2+4x^4+2x^6)+\frac{5}{14x}\mathrm{Li}_2(-x) \\
&-\frac{55}{49x}\mathrm{Li}_2(x)-\frac{75}{98x}\mathrm{Li}_2\Big(\frac{x-1}{x}\Big), \qquad x\leq 1-\Lambda^{-1}, \qquad (3\text{-}32)
\end{aligned}
$$

otherwise $p^{(1)}(-2;x)=p_{22}(-2;x)$ when $1+\Lambda^{-1}\leq x\leq 2$.For $x\ll 1$ we have:

$$
\begin{aligned}
p_{13}(-2;x,\Lambda) &\approx -\frac{4}{3}\Lambda+\frac{5\pi^2}{28x}+\mathcal{O}(x^0), \qquad (3\text{-}33)\\
p_{22}(-2;x,\Lambda) &\approx \frac{4}{3}\Lambda+\frac{75\pi^2}{196x}+\mathcal{O}(x^0), \qquad (3\text{-}34)\\
p^{(1)}(-2;x) &\approx \frac{55\pi^2}{98x}+\mathcal{O}(x^0). \qquad (3\text{-}35)
\end{aligned}
$$

3.2. One-Loop Smoothed Variance and Average Two-point Correlation Function

Using the results of the previous section for the power spectrum, we can calculate the 1-loop corrections to the variance and average two-point function, Eqs. (2-13, 2-12). We focus on the corresponding 1-loop amplitudes $s^{(1)}$ and $x^{(1)}$ defined in Eqs. (2-20, 2-21). From (2-21), (3-1), and (3-2) we can write:

$$
s^{(1)}(n;k_cR)\equiv\frac{(k_cR)^{2n+3}}{4[\Delta I_\sigma(n,k_cR,\Lambda)]^2}\int_0^{2k_cR}p^{(1)}(n;u(k_cR)^{-1},\Lambda)\;W^2(u)\;u^2du, \qquad (3\text{-}36a)
$$

$$
x^{(1)}(n;k_cR)\equiv\frac{(k_cR)^{2n+3}}{4[\Delta I_\xi(n,k_cR,\Lambda)]^2}\int_0^{2k_cR}p^{(1)}(n;u(k_cR)^{-1},\Lambda)\;W(u)\;u^2du, \qquad (3\text{-}36b)
$$

where $\Delta I_\sigma(n,k_cR,\Lambda)\equiv I_\sigma(n,k_cR)-I_\sigma(n,\epsilon R)$ and similarly for ΔI_ξ, with

$$I_\sigma(n,z) \equiv \int_0^z u^{n+2}\, W^2(u)\, du, \tag{3-37a}$$

$$I_\xi(n,z) \equiv \int_0^z u^{n+2}\, W(u)\, du. \tag{3-37b}$$

In Appendix A we present analytic results for I_σ and I_ξ with top-hat and Gaussian smoothing.

In Figs. 7 - 10, we show results for $s^{(1)}$ and $x^{(1)}$ for top-hat and Gaussian smoothing, based on numerical integration of Eq. (3-36). Similar results for $s^{(1)}$ for the Gaussian window function were presented by Łokas et al. (1995); comparison with our results shows very good agreement for scales such that $k_cR \gtrsim 2$. However, in the limit $k_cR \to 0$, they apparently find $s^{(1)} \approx 0$, instead of recovering the unsmoothed values reported in Scoccimarro & Frieman (1996) and in conflict with our results shown here. The source of their error may have been to replace $2k_cR$ by k_cR in the upper limit of integration in Eq. (3-36a); we found we could approximately reproduce their results with this change.

From Eqs. (3-36), one can analytically calculate $s^{(1)}$ and $x^{(1)}$ in the limit $k_cR \gg 1$ by asymptotic expansion in $1/k_cR$: for large k_cR, all we need is the behavior of $p^{(1)}(n;x,\Lambda)$ for small x given in the previous section. For $n=-2$ we have:

$$s^{(1)}(-2; k_cR \gg 1) \approx s^{(1)}(-2;\infty) = \frac{55\pi^2}{392}\frac{I_\sigma(-1,\infty)}{[I_\sigma(-2,\infty)]^2}, \tag{3-38}$$

where we used Eqs. (3-35) and (3-37a). An identical expression holds for $x^{(1)}$ upon replacing I_σ's by I_ξ's. Using the results in Appendix A, we find for *top-hat smoothing*:

$$s^{(1)}_{\rm TH}(-2;\infty) = \frac{1375}{1568} \approx 0.877, \tag{3-39}$$

$$x^{(1)}_{\rm TH}(-2;\infty) = \frac{110}{147} \approx 0.748. \tag{3-40}$$

For *Gaussian smoothing* we find

$$s^{(1)}_{\rm G}(-2;\infty) = x^{(1)}_{\rm G}(-2;\infty) = \frac{55\pi}{196} \approx 0.882 \tag{3-41}$$

in good agreement with the numerical results of Łokas et al. (1995), who found $s^{(1)}_{\rm G}(-2;\infty) \simeq 0.86$. Comparing these analytic results to Fig. 7, we see excellent agreement except for $x^{(1)}_{\rm TH}$,

which oscillates around the value given by Eq. (3-40). The reason for these oscillations can be partially understood from Eq. (3-38), using the results in Appendix A for finite k_cR. The behavior of $x^{(1)}_{\rm TH}$ is also due in part to the fact that smoothing with one top-hat window allows small-scale power in $p^{(1)}(n;x,\Lambda)$ to 'leak in' to the average correlation function, while (3-38) assumes that only the large-scale power contributes. For this reason, in the following we will give analytical results only for Gaussian smoothing.

For $n=-1$, using Eqs. (3-28) and (3-37a) we have:

$$s^{(1)}(-1;k_cR\gg 1) = \frac{3068}{11025}\frac{I_\sigma(1,\infty)}{[I_\sigma(-1,\infty)]^2}+\frac{244}{315}\int_0^\infty W^2(u)u^3\ln u\ du-\frac{61}{315}\frac{I_\sigma(1,\infty)}{[I_\sigma(-1,\infty)]^2} \times\ln(k_cR) \quad (3\text{-}42)$$

and similarly for $x^{(1)}$. Using Gaussian smoothing we find:

$$s^{(1)}_{\rm G}(-1;k_cR\gg 1) = \frac{6136}{11025}+\frac{61}{315}(1-\gamma_e)-\frac{122}{315}\ln(k_cR)\approx 0.638-0.387\ln(k_cR), \quad (3\text{-}43)$$

$$x^{(1)}_{\rm G}(-1;k_cR\gg 1) = \frac{6136}{11025}+\frac{61}{315}(1-\gamma_e+\ln 2)-\frac{122}{315}\ln(k_cR)\approx 0.773-0.387\ln(k_cR) \quad (3\text{-}44)$$

where $\gamma_e\simeq 0.577216...$ is the Euler-Mascheroni constant. Eqs. (3-43) and (3-44) are plotted as the dot-dashed curves in Fig. 8, which shows the excellent agreement with the results from the full numerical integration at large k_cR.

For $n=0$, one must include the next to leading order term at small x in $p^{(1)}(0;x,\Lambda)$, since this gives rise to a constant term in the 1-loop coefficients. We have:

$$p^{(1)}(0;x)\approx -\frac{244}{315}x^2+\frac{20\pi^2}{147}x^3+\mathcal{O}(x^4), \quad (3\text{-}45)$$

which gives (see dot-dashed curves in Fig. 9):

$$s^{(1)}_{\rm G}(0;k_cR\gg 1) = \frac{80\pi}{147}-\frac{122}{105\sqrt{\pi}}\ k_cR\approx 1.710-0.655\ k_cR, \quad (3\text{-}46)$$

$$x^{(1)}_{\rm G}(0;k_cR\gg 1) = \frac{80\pi}{147}-\frac{61}{105}\sqrt{\frac{2}{\pi}}\ k_cR\approx 1.710-0.464\ k_cR. \quad (3\text{-}47)$$

Similarly, for $n = 1$, we need the expansion:

$$p^{(1)}(1;x) \approx -\frac{122}{315}x^3 + \frac{18}{49}x^4 - \Big(\frac{4973}{22050} + \frac{16}{105}\ln x\Big)\ x^5 + \mathcal{O}(x^6), \tag{3-48}$$

which leads to (see Fig. 10):

$$\begin{aligned} s_{\rm G}^{(1)}(1;k_cR \gg 1) &= -\frac{4973}{7350} - \frac{4}{105}(11 - 6\gamma_e) + \frac{16}{35}\ln(k_cR) + \frac{135\sqrt{\pi}}{392}k_cR - \frac{122}{315}(k_cR)^2 \\ &\approx -0.964 + 0.457\ln(k_cR) + 0.610\ k_cR - 0.387\ (k_cR)^2, \end{aligned} \tag{3-49}$$

$$\begin{aligned} x_{\rm G}^{(1)}(1;k_cR \gg 1) &= -\frac{4973}{7350} - \frac{4}{105}(11 - 6\gamma_e + 6\ln 2) + \frac{16}{35}\ln(k_cR) + \frac{135}{392}\sqrt{\frac{\pi}{2}}k_cR \\ &\quad -\frac{61}{315}(k_cR)^2 \approx -1.122 + 0.457\ln(k_cR) + 0.432\ k_cR - 0.194\ (k_cR)^2. \end{aligned} \tag{3-50}$$

Note that the 1-loop coefficients are scale-dependent for $n \geq -1$; this is an indication of the breaking of self-similarity, as we discuss next. (A similar analysis to that above can be carried out for the 1-loop corrections in the Zel'dovich approximation, but details will not be given here.)

4. Self-Similarity and Perturbation Theory

4.1. Self-Similar Solutions

Since there is no preferred scale in the dynamics of a self-gravitating pressureless perfect fluid in an Einstein-de Sitter universe, Eqns. (2-1) admit self-similar solutions (see Peebles 1980). This means that the cosmological fields should scale with a self-similarity variable, given appropriate initial conditions: knowing the fields at a given time completely specifies their evolution. We can search for the appropriate self-similarity transformation by rewriting the fields as

$$\delta(\mathbf{x},\tau) \equiv \chi(\mathbf{y}), \tag{4-1a}$$

$$\mathbf{v}(\mathbf{x},\tau) \equiv \tau^{\mu}\mathbf{u}(\mathbf{y}), \tag{4-1b}$$

$$\Phi(\mathbf{x},\tau) \equiv \tau^{\gamma}\varphi(\mathbf{y}), \tag{4-1c}$$

where $\mathbf{y} \equiv \mathbf{x}/\tau^\nu$ is the similarity variable. Self-similarity is obeyed if we can rewrite Eqs. (2-1) in terms of $\mathbf{y}$ only; this condition determines the indices μ, γ, and ν. Note that the term $1 + \delta(\mathbf{x}, \tau)$ in the continuity equation (2-1a) precludes a power of τ prefactor in Eq. (4-1a). Substituting the ansatz Eq. (4-1) into Eq. (2-1a) and equating powers of τ we get the condition

$$\mu = \nu - 1, \tag{4-2}$$

whereas the Poisson equation Eq. (2-1c) gives:

$$\gamma = 2(\nu - 1). \tag{4-3}$$

These two conditions in turn guarantee that the Euler equation obeys self-similar evolution. The index ν can be determined in terms of the spectral index n of the linear power spectrum: Eq. (4-1a) implies that the two-point correlation function obeys the self-similar scaling

$$\xi(x, \tau) \equiv \Xi(x\tau^{-\nu}), \tag{4-4}$$

which upon Fourier transformation gives for the power spectrum

$$P(k, \tau) \equiv \tau^{3\nu}\ \mathcal{P}(k\tau^\nu). \tag{4-5}$$

On the other hand, in the linear regime, for a power-law initial power spectrum with spectral index n in an Einstein-de Sitter universe, $P_{11}(k, \tau) \sim \tau^4 k^n$; equating this with (4-5) fixes the remaining parameter in the similarity transformation,

$$\nu = \frac{4}{n + 3}, \tag{4-6}$$

(A more general derivation of (4-6) starts from the BBGKY hierarchy of equations for the phase space particle distribution functions, Davis & Peebles 1977.) Using these results, the equations of motion (2-1) can be rewritten in self-similar form:

$$\nu\mathbf{y} \cdot \hat{\nabla}\chi(\mathbf{y}) - \hat{\nabla} \cdot \{[1 + \chi(\mathbf{y})]\mathbf{u}(\mathbf{y})\} = 0, \tag{4-7a}$$

$$\nu\mathbf{y} \cdot \hat{\nabla}\mathbf{u}(\mathbf{y}) - (1 + \nu)\mathbf{u}(\mathbf{y}) - [\mathbf{u}(\mathbf{y}) \cdot \hat{\nabla}]\mathbf{u}(\mathbf{y}) = \hat{\nabla}\varphi(\mathbf{y}), \tag{4-7b}$$

$$\hat{\nabla}^2\varphi(\mathbf{y}) = 6\chi(\mathbf{y}), \tag{4-7c}$$

where $\hat{\nabla} \equiv \partial/\partial\mathbf{y}$. The solutions of these equations in the linear regime are $\chi(\mathbf{y}) \propto y^\zeta$ with $\zeta = -2/\nu, 3/\nu$, which correspond to the well-known linear growing and decaying modes, $\delta_1 \propto a, a^{-3/2}$. The condition of self-similar evolution also fixes the spatial dependence of the fields, e.g., $\delta_1(\mathbf{x}) \propto x^{-2/\nu}$ for the growing mode. However, we generally consider the density and velocity fields to be random fields, on which we impose initial conditions only *statistically*, e.g., by specifying the linear power spectrum for Gaussian initial conditions. A particular realization of the ensemble of initial conditions will not obey this spatial scaling, so the cosmological fields themselves will not be self-similar (Jain & Bertschinger 1995). Since NLCPT is built from linear solutions, the same conclusion applies to the expansions given by Eq. (2-5), which are not self-similar (except when the spatial dependence is fixed as above). Nevertheless, in some cases the *statistical* quantities of interest, such as the power spectrum, variance, and two-point correlation function, may exhibit self-similar scaling even if the fields in a given realization do not. We now consider the conditions under which this happens in perturbation theory.

4.2. Self-Similarity and Linear Perturbation Theory

The introduction of fixed (time-independent) cutoff scales ϵ and k_c in the linear power spectrum (3-1) breaks self-similarity, because they do not scale with the self-similarity variable $ka^{2/(n+3)}$ (the Fourier space analog of y). The extent to which one can take the limits $\epsilon \to 0$ and $k_c \to \infty$ will determine whether the statistical properties of the density field obey self-similar scaling. In the absence of cutoffs, the only physical scale that can be defined from the power spectrum is the correlation length, R_0, defined by:

$$\sigma^2(R_0) = \int P(k,\tau)W^2(kR_0)d^3k \equiv 1. \tag{4-8}$$

In linear perturbation theory, for scale-free initial conditions, one finds $R_0 \propto a^{2/(n+3)}$, which has the right time dependence to build the self-similarity variable. Consequently, in the *absence* of cutoffs, statistical quantities in linear theory evolve self-similarly with R_0, and we can write, e.g., (see Eqs. (4-4) and (4-5)):

$$\xi_\ell(r,\tau) \equiv \Xi_\ell(r/R_0), \tag{4-9}$$

$$R_0^{-3} P_{11}(k,\tau) \equiv \mathcal{P}_{11}(kR_0). \tag{4-10}$$

The presence of cutoffs in the initial spectrum changes this situation. From Eq. (3-1) we have

$$\begin{aligned} R_0^{n+3} &= 4\pi A a^2 \int_{\epsilon R_0}^{k_c R_0} \kappa^{n+2} W^2(\kappa) d\kappa \equiv 4\pi A a^2 [I_\sigma(n, k_c R_0) - I_\sigma(n, \epsilon R_0)] \\ &\equiv 4\pi A a^2 \Delta I_\sigma(n, k_c R_0, \Lambda), \end{aligned} \tag{4-11}$$

and R_0 will not scale as $a^{2/(n+3)}$ unless $\Delta I_\sigma(n, k_c R_0, \Lambda)$ is time independent. Before examining under which conditions this is true, it is useful to introduce another measure ℓ_0 of the correlation length, defined in terms of the volume-averaged correlation function,

$$\bar{\xi}(\ell_0) = \int P(k,\tau) W(k\ell_0) d^3k \equiv 1, \tag{4-12}$$

and therefore:

$$\ell_0^{n+3} = 4\pi A a^2 \int_{\epsilon \ell_0}^{k_c \ell_0} \kappa^{n+2} W(\kappa) d\kappa \equiv 4\pi A a^2 [I_\xi(n, k_c \ell_0) - I_\xi(n, \epsilon \ell_0)] \equiv 4\pi A a^2 \Delta I_\xi(n, k_c \ell_0, \Lambda). \tag{4-13}$$

Note that R_0 and ℓ_0 both differ slightly from the conventional definition of the correlation length, r_0, in terms of the two-point correlation function, $\xi(r_0) \equiv 1$.

A necessary condition for self-similarity in the variable R_0 (ℓ_0) is the convergence of the integrals ΔI_σ (ΔI_ξ) for small and large κ (where κ denotes kR_0 ($k\ell_0$)); otherwise these quantities would be sensitive to the cutoffs and consequently time dependent. From Eqs. (4-11) and (4-13), in order for the correlation length to scale self-similarly in linear theory, we must have *at least* the following conditions:

1. For a Gaussian filter, since $W(\kappa) \approx 1$ when $\kappa \to 0$, convergence in the infrared (small κ) requires $n > -3$. Convergence in the ultraviolet (large κ) is achieved for any n.

2. For a top-hat filter, convergence in the infrared requires $n > -3$. Since $W_{\rm TH}(\kappa) \approx \kappa^{-2}$ as $\kappa \to \infty$, convergence in the ultraviolet requires $n < 1$ in Eq. (4-11) and $n < -1$ in Eq. (4-13).

Note the dependence of these conditions on the local averaging scheme (top-hat vs. Gaussian) and the type of statistics (variance vs. average correlation function).

While these conditions guarantee convergence of $\Delta I_{\sigma,\xi}$, they do not test the constancy of these quantities for different choices of parameters. In Figs. 11 - 14, we show $\Delta I_{\sigma,\xi}(n, k_c R_0, \Lambda)$ for $\Lambda \equiv k_c/\epsilon = 10^2, 10^3, \infty$, as a function of $k_c R_0$ for spectral indices $n = -2, -1, 0, 1$. These finite values of Λ are comparable to the dynamic range currently achievable in N-body simulations. By definition, $k_c R_0$ measures the ratio of the correlation length to the small scale cutoff of the linear power spectrum. Therefore, in the region $k_c R_0 \approx 1$, the evolution of the correlation length is strongly affected by the cutoff k_c, and the $\Delta I_{\sigma,\xi}$ drop precipitously. By the time the correlation length has evolved to $k_c R_0 \gtrsim 3$, however, $\Delta I_{\sigma,\xi}$ reach their no-cutoff limits (in the cases where they converge). On the other hand, when $k_c R_0 \approx \Lambda$, i.e., $R_0 \approx \epsilon^{-1}$, the correlation length reaches the large-scale cutoff, and $\Delta I_{\sigma,\xi}$ again drops. This behavior is more dramatic as n decreases (and therefore strongest for $n = -2$) due to the increase in large-scale power. As expected from the discussion above, the definition of the correlation length using Gaussian smoothing displays self-similar evolution over a longer time interval than the other possibilities, with top-hat smoothing becoming notoriously worse as n increases.

The behavior of statistical quantities in linear perturbation theory with respect to self-similarity is determined directly from these considerations. We can write the linear power spectrum as (see Eq. (4-10)):

$$\mathcal{P}_{11}(kR_0, k_c R_0, \Lambda) \equiv \frac{(kR_0)^n}{4\pi \Delta I(n, k_c R_0, \Lambda)}, \tag{4-14}$$

where ΔI depends on the local averaging scheme and statistical quantity used to define the correlation length, and $kR_0 \ll 1$ in the linear regime. Unless otherwise noted, for power spectrum calculations we will use the choice in Eq. (4-11), i.e., R_0, with Gaussian smoothing. For the variance and average correlation function we have

$$\sigma^2_\ell(R/R_0, k_c R_0, \Lambda) \equiv \frac{\Delta I_\sigma(n, k_c R, \Lambda)}{\Delta I_\sigma(n, k_c R_0, \Lambda)} \left(\frac{R}{R_0}\right)^{-(n+3)}, \tag{4-15}$$

$$\bar{\xi}_\ell(R/R_0, k_c R_0, \Lambda) \equiv \frac{\Delta I_\xi(n, k_c R, \Lambda)}{\Delta I_\xi(n, k_c R_0, \Lambda)} \left(\frac{R}{R_0}\right)^{-(n+3)}. \tag{4-16}$$

Now the question is under what conditions are the statistics self-similar in the variables kR_0 (for the power spectrum) and R/R_0 (variance and average correlation function). In the

regime $R \gg R_0$ (where linear theory is valid) and

$$3 \lesssim k_c R_0 \ll k_c R \ll \Lambda, \tag{4-17}$$

Figs. 11 - 14 show that ΔI is approximately constant. Provided the conditions on n stated above hold, in this regime kR_0 and R/R_0 are self-similar variables: in linear perturbation theory, the power spectrum scales as

$$\mathcal{P}_{11}(kR_0, k_c R_0, \Lambda) \approx \frac{(kR_0)^n}{2\pi\Gamma\left(\frac{n+3}{2}\right)}, \tag{4-18a}$$

(see Eq. (A13)), and

$$\sigma_\ell^2(R/R_0, k_c R_0, \Lambda) \approx \bar{\xi}_\ell(R/R_0, k_c R_0, \Lambda) \approx \left(\frac{R}{R_0}\right)^{-(n+3)}. \tag{4-18b}$$

Note that, for top-hat smoothing, the requirement of self-similarity of the statistical quantities is in practice less restrictive than the requirement that R_0 or ℓ_0 scale self-similarly. For example, although ℓ_0, defined from top-hat smoothing, requires $n \lesssim -1$ to scale self-similarly, the average correlation function for $n = 1$ *does* scale self-similarly, i.e., it depends on R/R_0 only, in the regime given by Eq. (4-17),

$$\bar{\xi}_\ell(R/R_0, k_c R_0, \Lambda) \approx \left(\frac{R}{R_0}\right)^{-3}, \tag{4-19}$$

(see Eq. (A8d)) where we have averaged over oscillatory behavior. However, it does not obey the "expected" $\bar{\xi}_\ell(R/R_0, k_c R_0, \Lambda) \approx (R/R_0)^{-4}$ scaling. This trend appears to be seen in the results from high-resolution scale-free N-body simulations (Colombi et al. 1995).

4.3. Self-Similarity and Non-Linear Perturbation Theory

We have examined the conditions under which linear perturbation theory obeys self-similar scaling. We now turn to the question of whether loop corrections in NLCPT affect self-similar scaling.

Using the results of the previous section and Eq. (3-2), we can write the power spectrum up to 1-loop corrections as:

$$\mathcal{P}(kR_0, k_cR_0, \Lambda) \equiv \frac{(kR_0)^n}{4\pi\Delta I_\sigma(n, k_cR_0, \Lambda)} + \frac{(k_cR_0)^{2n+3}}{16\pi[\Delta I_\sigma(n, k_cR_0, \Lambda)]^2}\, p^{(1)}(n; k/k_c, \Lambda), \qquad (4\text{-}20)$$

where $kR_0 \lesssim 1$ in the weakly non-linear regime. Self-similarity is maintained at the 1-loop level if, in the scaling regime given by

$$kR_0 \lesssim 1 \ll k_cR_0 \ll \Lambda, \qquad (4\text{-}21)$$

the dependence of $\mathcal{P}(kR_0, k_cR_0, \Lambda)$ on k_cR_0 and Λ is negligible, that is, if

$$p^{(1)}(n; k/k_c \to 0, \Lambda \to \infty) \approx a_n \left(\frac{k}{k_c}\right)^{2n+3}, \qquad (4\text{-}22)$$

with a_n some constant which depends only on the spectral index n. From the results of Section 3.1, we see that this condition is only satisfied when $n = -2$. In this case we have (see Eq. (3-35)):

$$\mathcal{P}(kR_0; n = -2) \approx \frac{1}{2\pi^{3/2}}(kR_0)^{-2} + \frac{55}{392}(kR_0)^{-1}, \qquad (4\text{-}23)$$

which takes the self-similar form. For $n = -1$, 1-loop diagrams yield logarithmic k_c-dependent corrections to self-similar scaling (see Eq. (3-28)),

$$\mathcal{P}(kR_0, k_cR_0) \approx \frac{1}{2\pi}(kR_0)^{-1} + \frac{16}{11025\pi}\ (kR_0)\ \left[3068 + 2135 \ln\left(\frac{k}{k_c}\right)\right]. \qquad (4\text{-}24)$$

The results for $n = 0, 1$ show a stronger power law breaking of self-similarity (see Eqs. (3-19) and (3-12)):

$$\mathcal{P}(kR_0, k_cR_0) \approx \frac{(kR_0)^n}{2\pi\ \Gamma\left(\frac{n+3}{2}\right)} - \frac{61\ (kR_0)^{2n+3}}{315\pi(n+1)\ \Gamma^2\left(\frac{n+3}{2}\right)}\ \left(\frac{k}{k_c}\right)^{\eta}, \qquad (4\text{-}25)$$

where $\eta = -(n+1)$ is an exponent which measures the deviation from self-similar scaling, generally known as *the anomalous dimension* in the theory of critical phenomena (Goldenfeld 1992, Barenblatt 1979). A visual summary of these results is given in the next subsection, where we compare 1-loop NLCPT to the universal scaling hypothesis first proposed by

Hamilton et al. (1991). For the variance and average two-point correlation function, self-similarity breaking means that, in the expected scaling region given by Eq. (4-17), the 1-loop coefficients $s^{(1)}$ and $x^{(1)}$ (see Eq. (2-20)) are scale-dependent; in Sec. 3.2, we found this to be the case when $n \geq -1$. Thus, for $n \geq -1$, we find generally that self-similarity is broken in perturbation theory by the first non-linear (1-loop) corrections to the power spectrum.

Our conclusions about self-similarity in NLCPT differ substantially from those of Jain & Bertschinger (1995). The primary difference stems from the fact that they take the small scale cutoff in the linear power spectrum, k_c, to be *time dependent* in comoving coordinates. They choose k_c to scale as the inverse correlation length, i.e., they fix $k_c R_0 \approx 1$ throughout the evolution. Their rationale for this is plausible: since NLCPT is expected to break down at scales below the correlation length R_0, within the framework of perturbation theory one should perhaps restrict contributions to the power spectrum to scales larger than R_0. Since R_0 depends on time, the cutoff of the linear power spectrum must be chosen to scale as $1/R_0$ in order to satisfy this requirement at all times. Using this condition on $k_c R_0$, they correctly conclude that the power spectrum evolves self-similarly (to any order in NLCPT), *provided* there are no infrared divergences. At 1-loop, we can see this directly from Eq. (4-20): if $k_c R_0 \equiv 1$ and if $p^{(1)}$ is convergent in the limit $\Lambda \to \infty$, then the power spectrum depends only on kR_0 and therefore obeys self-similarity. However, while Jain & Bertschinger did show that leading infrared divergences cancel as loop momenta become vanishingly small, they did not compute loop corrections to the power spectrum explicitly. In fact, as we saw above, for $n = -1, -2$, $p^{(1)}$ develops a singularity at $k = k_c$, and the limit $\Lambda \to \infty$ does not exist. This necessarily introduces a dependence of the 1-loop power spectrum on $\Lambda = k_c/\epsilon$. As a result, even if $k_c R_0$ is held fixed, self-similarity is broken, *unless* ϵ is *also* assumed to scale with R_0 as k_c does; we do not know of any arguments (analogous to that above) that would require ϵ to scale this way.

We take a different viewpoint on this question. As Jain & Bertschinger note, it is not surprising that choosing $k_c R_0 \approx 1$ throughout the evolution leads to self-similarity, since one is identifying the cutoff scale with the correlation length. In fact, this choice can be characterized as artificially *introducing* self-similarity into the problem via the initial conditions. Here, we are rather interested in the question of whether self-similarity arises from the dynamical evolution over some range of scales far from the cutoffs (e.g., that given by Eq. (4-21)) when the initial conditions are not exactly scale-free. The basis of perturbation theory is the *assumption* that the statistical evolution of the large-scale fields can be determined perturbatively even when the density and velocity fields are highly non-linear on the smallest scales. Therefore, when $k_c R_0 > 1$, one should include perturbative contributions from scales below R_0 and see whether the results are sensible and/or self-similar, rather than continuously remove this power transfer by hand on the grounds that

the theory is expected to break down. This assumption of course *will* break down at late enough times and/or small enough scales, but it can be *tested*, and its range of validity quantified, by checking its predictions against numerical simulations. *A fortiori*, our choice of fixed comoving cutoffs is close to the conditions in (scale-free) N-body simulations, where infrared and ultraviolet cutoffs are imposed by the box size and the grid scale, both of which are fixed in comoving coordinates. [This is not strictly true in the later stages of evolution for high-resolution codes (such as P^3M and tree codes), where the small-scale cutoff is eventually set by the mean interparticle distance; when the small-scale clustering stabilizes, this yields $k_c \propto a$, which, while not constant, has the *opposite* time dependence from the scaling needed for self-similarity, $k_c \propto a^{-2/(n+3)}$.]

We expect that in models with relatively more small-scale power, i.e., larger n, the basic assumption of NLCPT will have a smaller range of validity: the power being fed from small to large scales soon invalidates the perturbative approach. In fact, the stronger breaking of self-similarity we have found in NLCPT at larger n points to this conclusion, because scale-free N-body simulations exhibit self-similar scaling to very good accuracy for $n \gtrsim -(1-3)$. To assess this issue quantitatively, we now turn to a comparison of NLCPT predictions with the "universal" scaling observed in scale-free numerical simulations.

4.4. Comparison with Simulations: the Universal Scaling Hypothesis

The universal scaling hypothesis (Hamilton et al. 1991) asserts that the non-linear evolution of the average two-point correlation function can be obtained from its linear counterpart by a universal scaling relation. This relation has been derived empirically from the study of numerical simulations for scale-free and CDM power spectra, but its main features can be understood on physical grounds (Nityananda & Padmanabhan 1994). These results have been extended by Peacock & Dodds (1994) to a universal relation between linear and non-linear power spectra and by Jain et al. (1995) to include the dependence of the scaling relation on the spectral index n. In its current version, the universal scaling hypothesis for the dimensionless power spectrum,

$$\Delta(k) \equiv 4\pi k^3 P(k), \tag{4-26}$$

relates the linear (Δ_ℓ) to the non-linear evolved (Δ_e) spectrum via

$$\Delta_e(k_e) = B(n)\ \Phi[\Delta_\ell(k)/B(n)], \qquad k^3 \equiv \frac{k_e^3}{1+\Delta_e(k_e)}, \tag{4-27}$$

where the simulations are empirically fit by setting $B(n) = (1 + n/3)^{1.3}$ and

$$\Phi(z) = z \left(\frac{1 + 0.6z + z^2 - 0.2z^3 - 1.5z^{7/2} + z^4}{1 + 0.0037z^3} \right)^{1/2}. \tag{4-28}$$

The ansatz in Eq. (4-27) is equivalent to the hypothesis that the mean dimensionless pairwise velocity is a universal function of the average two-point correlation function (Hamilton et al. 1991, Nityananda & Padmanabhan 1994). Note that the linear spectrum is mapped to the non-linear spectrum at smaller scale ($k_e > k$), reflecting the fact that non-linearly evolving perturbations shrink in comoving coordinates. The specific relation between k and k_e in (4-27) can be obtained from the evolution equation for the average correlation function (conservation of pairs), according to which the mean number of neighbors within distance r_e of a particle is time independent if r_e decreases in time according to $r^3 \equiv r_e^3[1 + \bar{\xi}_e(r_e)]$; here r is a fixed scale, the radius of a sphere which encloses the same number of neighbors in the linear regime.

We now compare these expressions with the perturbative calculations of the previous sections. We can write the dimensionless power spectrum up to 1-loop corrections as (see Eq. (4-20)):

$$\Delta_e(kR_0, k_cR_0, \Lambda) \equiv \frac{(kR_0)^{n+3}}{\Delta I_\sigma(n, k_cR_0, \Lambda)} + \frac{(k_cR_0)^{2n+3}\ (kR_0)^3}{4[\Delta I_\sigma(n, k_cR_0, \Lambda)]^2}\ p^{(1)}(n; k/k_c, \Lambda). \tag{4-29}$$

In Fig. 15 we compare the 1-loop NLCPT relation between linear and non-linear dimensionless power spectra with the universal scaling hypothesis (USH) for spectral index $n = -2$. The different dotted curves correspond to the predictions of NLCPT for $k_cR_0 = 10^\alpha$, with $\alpha = 0.5 - 2$; since $3 \lesssim k_cR_0 \ll \Lambda = 10^3$, cutoff effects in the linear evolution of the correlation length are negligible [see Eq. (4-17) and Fig. (11)]. Each curve extends down to scales such that $(kR_0)_{max} \equiv 10^{\alpha - 1/10}$. The agreement between NLCPT and the USH (solid curve) is impressive all the way down to scales where $\Delta_e \approx 10$, far beyond the domain of linear perturbation theory (see also Łokas et al. (1995) for a comparison between NLCPT and N-body results for $n = -2$). For smaller scales than this, the 1-loop power spectrum overestimates the non-linear power spectrum. Note, however, that the turnover at $\Delta_e \approx 10$ in the USH curve marks the onset of the transition to the regime described by the stable clustering hypothesis, and therefore disagreement with NLCPT beyond this point is not surprising. The NLCPT curve for $\alpha = 2$ shows a slight disagreement with self-similarity at the large-scale end, which corresponds to the fact that, at this stage of evolution, these scales are not negligible compared to the size of the system. Otherwise, the agreement with

self-similarity is excellent. For comparison, we also present the perturbative results to 1-loop for the Zel'dovich approximation (ZA) for $k_c R_0 = 100$ (dot-dashed curve). The agreement between ZA and the USH is not very good, although the results of the N-body simulations of Jain et al. (1995) display a scatter comparable to the difference. In fact, their earlier (higher redshift) outputs seem to fit the ZA predictions shown here, suggesting that some of their scatter for $n = -2$ may be due to transients from the ZA initial conditions of the simulations.

In Figs. 16 - 18, we show the same comparison for spectral indices $n = -1, 0, 1$. As expected from the discussion in the previous sections and the fact that the USH is self-similar by construction, for $n \geq -1$ there is obvious disagreement between NCLPT and USH. This discord becomes more evident as time evolution proceeds (a change in the scale factor by Δa corresponds to $\Delta a \equiv 10^{(n+3)\Delta\alpha/3}$), as the scales considered decrease, or as the spectral index increases. The dotted curves that drop after reaching a maximum end close to the scale where the 1-loop corrections dominate over the tree-level contribution, driving Δ_e negative (this happens at $kR_0 < 1$). A similar conclusion regarding the disagreement between NLCPT and the USH has been recently noted by Bharadwaj (1995), who examined the hypothesis that the mean dimensionless pairwise velocity is a universal function of the average correlation function. From the analysis of the BBGKY hierarchy in the weakly non-linear regime, he showed that this hypothesis is not obeyed at the 1-loop level for linear power spectra $P_{11}(k) \propto k \exp(-k)$, consistent with our results for $n = 1$. In fact, we find that non-linear perturbation theory fares worse than linear theory for $n \gtrsim -1$.

A comparison of the USH with NLCPT to 1-loop has also been carried out by Łokas et al. (1995), who concluded, based on numerical calculations of the $s^{(1)}$ coefficients for Gaussian smoothing, that the agreement was good. Their main focus, however, was to understand whether non-linear evolution decreases or increases the growth rate of structure with respect to that predicted by linear perturbation theory. In this regard, NLCPT qualitatively agrees with the USH in the sense that both predict that the growth rates are increased over linear theory when $n = -2$ and decreased when $n \geq 0$ (with $n = -1$ showing marginal behavior). However, as we have seen, the *quantitative* agreement is poor for $n \geq -1$: the scale-dependence of the $s^{(1)}$ coefficients in NLCPT disagrees with that of the USH, which by self-similarity requires $s^{(1)} \approx$ const. in the scaling regime given by Eq. (4-21).

In fact, one can extract the $s^{(1)}$ coefficients predicted by the USH from Eqs. (4-27) and (4-28) by using a small-Δ_e expansion,

$$\Delta^{(1)} \approx \left[0.3 \left(\frac{3}{n+3}\right)^{1.3} - \left(\frac{n+3}{3}\right)\right] \Delta_\ell^2, \tag{4-30}$$

[compare to Eq. (4-29)]. Using Gaussian smoothing, this gives

$$s_{\rm G}^{(1)}({\rm USH}) \approx \frac{2\,\Gamma(n+3)}{\Gamma^2\left(\frac{n+3}{2}\right)}\left[0.3\,\left(\frac{3}{n+3}\right)^{1.3} - \left(\frac{n+3}{3}\right)\right], \tag{4-31}$$

which yields $s_{\rm G}^{(1)} \approx 0.58, -0.32, -3.56, -13.52$ for $n = -2, -1, 0, 1$ respectively. These results should be taken with caution, however, because the range over which the next-to-leading order term in the fitting formula (4-28) dominates is quite narrow (Jain et al. 1995) and therefore sensitive to uncertainties in the fitting formulae. To quantify this uncertainty, one can, for example, calculate $x_{\rm TH}^{(1)}$ for $n = -2$ from the result in Eq. (4-30), which gives $x_{\rm TH}^{(1)}(-2) \approx 0.50$; on the other hand, a more direct calculation from the fitting formula for the average correlation function (analogous to Eq. (4-28)) given in Jain et al. 1995 yields $x_{\rm TH}^{(1)}(-2) \approx 0.75$, in remarkable agreement with the perturbative result, Eq. (3-40). For $n = -1, 0, 1$, the USH fitting formula for the average correlation function yields $x_{\rm TH}^{(1)} \approx -0.04, -0.55, -0.98$. We also note that these results and Eq. (4-31) predict a similar behavior regarding the change of sign of the 1-loop corrections as n increases, as pointed out by Łokas et al. (1995).

4.4.1. Self-similarity via Dimensional Regularization

In the results presented so far, we imposed infrared and ultraviolet cutoffs on the initial power spectrum to obtain finite integrals. For $n = -2$, however, we have seen that the resulting 1-loop power spectrum in the scaling regime is independent of the cutoffs and thus self-similar; this suggests that in this case the loop corrections can be alternatively calculated without the need to employ cutoffs. In fact, if the spectral index is in the range $-3 \leq n < -1$, one can show that 1-loop NLCPT preserves self-similarity by considering $p^{(1)}$ in the no-cutoff limit and using dimensional regularization to regularize the required integrations (see Appendix B). Dimensional regularization is much simpler than the cutoff approach, because it obviates the need for complicated constraints on the angular integration variable [see Eq. (3-5)]. It also makes possible the analytic calculation for non-integer values of n.

In Fig. 19, we show $x_{\rm TH}^{(1)}$, derived via dimensional regularization for $-3 \leq n < -1$, and compare it with the predictions of the USH taken directly from the fitting formula for the average correlation function (labeled USH - ξ) and from the dimensionless power spectrum ansatz (USH - Δ). We see that the agreement is very good over most of this range. The NLCPT results diverge as $n \to -1$, as expected from the logarithmic divergence

found as $k_c \to \infty$ in the cutoff calculation. As $n \to -3$, the NLCPT result goes to the unsmoothed value $x^{(1)} = s^{(1)} = 4063/2205 \approx 1.843$ (Scoccimarro & Frieman 1996); this can be understood from the fact that large scale fluctuations become dominant and averaging over small scales has a negligible effect. (By contrast, the USH has a singularity at $n \to -3$ due to the way that the n-dependence is parametrized through $B(n)$ in the USH fitting formula; since the USH was extracted from simulations with $n \geq -2$, it should probably only be trusted in that range.) The linear part of the NLCPT curve is well described by an expansion about $n = -3$:

$$x^{(1)}_{\rm TH}(n;\infty) = \frac{4063}{2205} - \frac{3679}{2205}\,(n+3) \approx 1.843 - 1.168\,(n+3). \tag{4-32}$$

Similar computations can be carried out in NLCPT for Gaussian smoothing and for the smoothed $s^{(1)}$ coefficient; the results show essentially the same features as displayed in Fig. 19.

5. Summary and Conclusions

We have calculated the one-loop (first non-linear) corrections to the power spectrum, average two-point correlation function, and variance of the density field, including smoothing effects for top-hat and Gaussian filters, for scale-free Gaussian initial conditions. For the power spectrum, these results should replace the expressions given in Makino et al. (1992) for the p_{22} contribution on lengthscales smaller than the inverse ultraviolet cutoff of the linear spectrum ($k_c < k < 2k_c$). Our results for the one-loop corrections to the variance extend those of Łokas et al. (1995) to top-hat smoothing and correctly go over to the unsmoothed values found in Scoccimarro & Frieman (1996) when the smoothing radius approaches zero.

We found that, when formulated with "fixed" comoving cutoffs, non-linear perturbation theory beyond tree-level does not obey self-similar scaling when the spectral index $n \geq -1$. As a consequence, in this spectral range, NLCPT disagrees with the results of N-body simulations embodied in the self-similar universal scaling ansatz (USH). For $-3 < n < -1$, however, we found that one-loop corrections do obey self-similar scaling and are in excellent agreement with the USH down to lengthscales where the dimensionless power spectrum $\Delta_e(k) \simeq \sigma^2(R \sim 1/k) \approx 10$; below this scale, the N-body results make the transition to the highly non-perturbative regime described approximately by stable clustering.

We interpret the breaking of self-similarity for $n \geq -1$ as a signature of the breakdown of the fundamental assumption that the large-scale evolution of the density field can be calculated perturbatively when there are highly non-linear fluctuations on small scales. In this instance, self-similarity breaking can be thought of as arising from an ultraviolet divergence

in the 1-loop corrections as the small-scale cutoff k_c of the linear power spectrum goes to infinity. This problem is more severe as the spectral index n increases, which is the expected behavior due to the increase in small-scale power.

Since for $n \geq -1$, the relative power on small scales is large, the question arises of whether the disagreement between the perturbative results and numerical simulations is due to the breakdown of perturbation theory (as we argued above) or to the use of the single-stream approximation, which neglects the effects of pressure gradients due to velocity dispersion. When these effects are included, one expects that the anisotropic velocity dispersion (non-radial motions) associated with small-scale substructure can inhibit the collapse of large-scale perturbations—the "previrialization" effect (Davis & Peebles 1977, Evrard & Crone 1992, Łokas et al. 1995, Peebles 1990). In fact, as $n \to -1$ from below, $s^{(1)}$ changes sign and becomes negative, showing that such an effect is already present at some level in the single-stream approximation. In addition, the terms neglected in the single-stream approach have been included by Bharadwaj (1995), who nevertheless finds exactly the same results as in the single-stream approximation. Therefore, if velocity dispersion terms indeed become important, it appears that their effects cannot be treated perturbatively. This suggests that the interpretation given above is the correct one, i.e., for $n \geq -1$ the non-linear evolution of the density power spectrum is inherently non-perturbative, and perturbative methods are of little use.

Given the excellent agreement between 1-loop NLCPT and N-body results for $n \lesssim -1$, one is naturally led to ask whether this agreement can be improved upon, i.e., extended to smaller lengthscales, by going to next order (2-loop corrections). We regard this to be unlikely, since the USH suggests that the physical picture involved in this small-scale regime is well described by stable clustering, which cannot be obtained perturbatively starting from linear solutions. Another interesting question is whether the validity of loop corrections in NLCPT for higher order cumulants (such as the bispectrum, skewness, etc.) will follow the same pattern with spectral index. We will address this issue in future work.

We would like to thank S. Colombi, J. Fry, and R. Juszkiewicz for useful conversations. This research was supported in part by the DOE at Chicago and Fermilab and by NASA grant NAG5-2788 at Fermilab. After this paper was completed, we received a revised version of Łokas et al. 1995, which contains a number of improvements and corrections, made partly in response to our criticisms. They now agree with our numerical results for $s^{(1)}$ in the regime $k_c R \lesssim 1$, and they have reproduced our analytic expressions for $s^{(1)}(n; k_c R \gg 1)$, our Eqns.(3-39 - 3-49).

A. Expressions for I_σ and I_ξ

Recall the definitions given in the text (see Eqs. (3-37)) :

$$I_\sigma(n,z) \equiv \int_0^z u^{n+2}\ W^2(u)\ du, \tag{A1}$$

$$I_\xi(n,z) \equiv \int_0^z u^{n+2}\ W(u)\ du. \tag{A2}$$

Here we tabulate these integrals as a function of filter and spectral index.

A.1. Top-Hat Smoothing

$$\begin{aligned}
I_\sigma(-2,z) &= \frac{3}{10z^5}\Big[-3-5z^2+(3-z^2+2z^4)\cos(2z)+(6z+z^3)\sin(2z) \\
&\quad +4z^5\mathrm{Si}(2z)\Big], && \text{(A3a)}\\
I_\sigma(-1,z) &= \frac{9}{4}+\frac{9}{8z^4}\Big[-1-2z^2+\cos(2z)+2z\sin(2z)\Big], && \text{(A3b)}\\
I_\sigma(0,z) &= \frac{3}{2z^3}[-1-3z^2+(1+z^2)\cos(2z)+2z\sin(2z)+2z^3\mathrm{Si}(2z)], && \text{(A3c)}\\
I_\sigma(1,z) &= -\frac{9}{2}(1-\gamma_e-\ln 2)+\frac{9}{4z^2}[-1+\cos(2z)-2z^2\mathrm{Si}(2z)+2z^2\ln(z) \\
&\quad +2z\sin(2z)], && \text{(A3d)}
\end{aligned}$$

where $\mathrm{Si}(z)$ and $\mathrm{Ci}(z)$ denote the sine and cosine integrals, defined by

$$\begin{aligned}
\mathrm{Si}(z) &\equiv \int_0^z \frac{\sin(u)}{u}du, && \text{(A4)}\\
\mathrm{Ci}(z) &\equiv -\int_z^\infty \frac{\cos(u)}{u}du, && \text{(A5)}
\end{aligned}$$

and $\gamma_e \simeq 0.577216...$ is the Euler-Mascheroni constant. As $z \to \infty$, we have $\mathrm{Ci}(z) \to 0$ and $\mathrm{Si}(z) \to \pi/2$. Using the following expression of a top-hat filter in terms of Bessel functions:

$$W_{\rm TH}(u) = 3\sqrt{\frac{\pi}{2}}u^{-3/2}J_{3/2}(u), \tag{A6}$$

we have (for any n in the range $-3 < n < 1$):

$$I_\sigma(n,\infty) = 9\pi 2^{n-2}\frac{\Gamma(1-n)\Gamma[(n+3)/2]}{\Gamma^2(1-n/2)\Gamma[(5-n)/2]}, \tag{A7}$$

where $\Gamma(x)$ denotes the gamma function. For $I_\xi(n,z)$ we obtain:

$$I_\xi(-2,z) = \frac{3}{2}\left[\mathrm{Si}(z) + \frac{\cos(z)}{z} - \frac{\sin(z)}{z^2}\right], \tag{A8a}$$

$$I_\xi(-1,z) = 3[1-\sin(z)/z], \tag{A8b}$$

$$I_\xi(0,z) = 3[\mathrm{Si}(z) - \sin(z)], \tag{A8c}$$

$$I_\xi(1,z) = 3[2 - 2\cos(z) - z\sin(z)]. \tag{A8d}$$

Using Eq. (A6), we have ($-3 < n < 0$):

$$I_\xi(n,\infty) = 3\sqrt{\pi}2^n\frac{\Gamma[(n+3)/2]}{\Gamma(1-n/2)}. \tag{A9}$$

A.2. Gaussian Smoothing

$$I_\sigma(-2,z) = \frac{\sqrt{\pi}}{2}\mathrm{erf}(z) \tag{A10a}$$

$$I_\sigma(-1,z) = \frac{1}{2}[1-\exp(-z^2)] \tag{A10b}$$

$$I_\sigma(0,z) = \frac{\sqrt{\pi}}{4}\,\mathrm{erf}(z) - \frac{1}{2}z\exp(-z^2) \tag{A10c}$$

$$I_\sigma(1,z) = \frac{1}{2} - \frac{(1+z^2)}{2}\exp(-z^2) \tag{A10d}$$

where $\mathrm{erf}(z)$ denotes the error function,

$$\mathrm{erf}(z) \equiv \frac{2}{\sqrt{\pi}} \int_0^z \exp(-u^2) du, \tag{A11}$$

and for $I_\xi(n,z)$ we have:

$$I_\xi(n,z) = 2^{(n+3)/2}\ I_\sigma(n, z/\sqrt{2}). \tag{A12}$$

When $z \to \infty$ we obtain:

$$I_\sigma(n,\infty) = \frac{1}{2}\ \Gamma\left(\frac{n+3}{2}\right). \tag{A13}$$

B. Dimensional Regularization

To obtain the low-k behavior of the power spectrum for $n < -1$, one can use dimensional regularization to simplify considerably the calculations, and get one-loop coefficients such as $x^{(1)}(n;\infty)$ for n in the range $-3 < n < -1$. Since we are interested in the limit $k_c \to \infty$, all the integrals run from 0 to ∞, and divergences are regulated by changing the dimensionality d of space: we take $d = 3 + \epsilon$ and expand in $\epsilon \ll 1$. For power spectrum calculations, we need the following standard formula for dimensional-regularized integrals (Collins 1984):

$$\int \frac{d^d\mathbf{q}}{(q^2)^{\nu_1}[(\mathbf{k}-\mathbf{q})^2]^{\nu_2}} = \frac{\Gamma(d/2-\nu_1)\Gamma(d/2-\nu_2)\Gamma(\nu_1+\nu_2-d/2)}{\Gamma(\nu_1)\Gamma(\nu_2)\Gamma(d-\nu_1-\nu_2)}\ \pi^{d/2}\ k^{d-2\nu_1-2\nu_2}. \tag{B1}$$

When using this equation, divergences appear as poles in the gamma functions, which can be handled by the following expansion ($n = 0, 1, 2, \ldots$ and $\epsilon \to 0$):

$$\Gamma(-n+\epsilon) = \frac{(-1)^n}{n!}\left[\frac{1}{\epsilon} + \psi(n+1) + \frac{\epsilon}{2}\left(\frac{\pi^2}{3} + \psi^2(n+1) - \psi'(n+1)\right) + \mathcal{O}(\epsilon^2)\right], \tag{B2}$$

where $\psi(x) \equiv d\ln\Gamma(x)/dx$ and

$$\psi(n+1) = 1 + \frac{1}{2} + \ldots + \frac{1}{n} - \gamma_e, \tag{B3a}$$

$$\psi'(n+1) = \frac{\pi^2}{6} - \sum_{k=1}^{n} \frac{1}{k^2}, \tag{B3b}$$

with $\psi(1) = -\gamma_e$ and $\psi'(1) = \pi^2/6$. We can write the one-loop power spectrum as (see Eq. (2-19)):

$$P^{(1)}(k,\tau;n) = A^2 a^4(\tau) \int d^d\mathbf{q}\; q^n \left(2|\mathbf{k}-\mathbf{q}|^n\; [F_2^{(s)}(\mathbf{k}-\mathbf{q},\mathbf{q})]^2 + 6k^n\; F_3^{(s)}(\mathbf{k},\mathbf{q},-\mathbf{q})\right). \quad \text{(B4)}$$

In the numerators of the integrands, we can use the relation $2\;\mathbf{q}\cdot\mathbf{k} = -(\mathbf{k}-\mathbf{q})^2 + k^2 + q^2$ to rewrite Eq. (B4) exclusively in terms of integrals of the form (B1). The resulting 1-loop power spectrum contributions for $-3 < n < -1$ are

$$\begin{aligned} P_{22}(k,\tau;n) \;=\; & \left(\frac{\Gamma(5/2-n)\Gamma^2[(n-1)/2]}{2\Gamma^2(2-n/2)\Gamma(n-1)} + \frac{3\Gamma(3/2-n)\Gamma[(n-1)/2]\Gamma[(n+1)/2]}{\Gamma(1-n/2)\Gamma(2-n/2)\Gamma(n)}\right. \\ & + \frac{29\Gamma(1/2-n)\Gamma^2[(n+1)/2]}{4\Gamma^2[1-n/2]\Gamma(n+1)} + \frac{11\Gamma(1/2-n)\Gamma[(n-1)/2]\Gamma[(n+3)/2]}{4\Gamma(2-n/2)\Gamma(-n/2)\Gamma(n+1)} \\ & - \frac{15\Gamma(-1/2-n)\Gamma[(n-1)/2]\Gamma[(n+5)/2]}{2\Gamma(-1-n/2)\Gamma(2-n/2)\Gamma(n+2)} + \frac{15\Gamma(-1/2-n)\Gamma[(n+1)/2]}{2\Gamma(1-n/2)\Gamma(-n/2)} \\ & \times\frac{\Gamma[(n+3)/2]}{\Gamma(n+2)} - \frac{25\Gamma(-3/2-n)\Gamma[(n+1)/2]\Gamma[(n+5)/2]}{\Gamma(-1-n/2)\Gamma(1-n/2)\Gamma(n+3)} + \frac{25\Gamma(-3/2-n)}{4\Gamma(-2-n/2)} \\ & \times\frac{\Gamma[(n-1)/2]\Gamma[(n+7)/2]}{\Gamma(2-n/2)\Gamma(n+3)} + \left.\frac{75\Gamma(-3/2-n)\Gamma^2[(n+3)/2]}{4\Gamma^2[-n/2]\Gamma(n+3)}\right) \frac{\pi^{3/2}A^2a^4(\tau)}{49} \\ & \times k^{2n+3}, \end{aligned} \quad \text{(B5)}$$

$$\begin{aligned} P_{13}(k,\tau;n) \;=\; & \left(-\frac{\Gamma[(n+1)/2]\Gamma[(1-n)/2]}{84\Gamma(1-n/2)\Gamma(1+n/2)} - \frac{19\Gamma[-(n+3)/2]\Gamma[(n+5)/2]}{84\Gamma(-1-n/2)\Gamma(3+n/2)}\right. \\ & + \frac{\Gamma[-(n+5)/2]\Gamma[(n+7)/2]}{12\Gamma[-2-n/2]\Gamma(4+n/2)} + \frac{5\Gamma[-(n+1)/2]\Gamma[(n+3)/2]}{28\Gamma(2+n/2)\Gamma(-n/2)} \\ & \left. - \frac{\Gamma[(n-1)/2]\Gamma[(3-n)/2]}{42\Gamma(2-n/2)\Gamma(n/2)}\right) \pi^2 A^2 a^4(\tau)\; k^{2n+3}. \end{aligned} \quad \text{(B6)}$$

Note that this implies that $P^{(1)} \propto k^{2n+3}$, as required by self-similarity.

REFERENCES

Barenblatt, G. I. 1979, *Similarity, Self-Similarity, and Intermediate Asymptotics*, Consultants Bureau, New York (1979).

Baugh, C. M. & Efstathiou, G. 1994, MNRAS, 270, 183

Baugh, C. M., Gaztañaga, E., & Efstathiou, G. 1995, MNRAS 274, 1049

Bernardeau, F. 1994, A&A 291, 697

Bertschinger, E. & Gelb, J. 1991, Comp. in Physics, 5, 164

Bharadwaj, S. 1995, preprint, astro-ph/9511085

Coles, P. 1990, MNRAS, 243, 171

Colombi, S., Bouchet, F. R., & Hernquist, L. 1995, preprint, astro-ph/9508142

Collins, J. C. 1984, *Renormalization*, (Cambridge: Cambridge University Press)

Davis, M. & Peebles, P. J. E. 1977, ApJS, 34, 25

Efstathiou, G., Frenk, C. S., White, S. D. M., & Davis, M. 1988, MNRAS, 235, 715

Evrard A. E. & Crone M. M. 1992, ApJ, 394, L1

Fry, J. N. 1984, ApJ, 279, 499

Fry, J. N. 1994, ApJ, 412, 21

Gaztañaga, E. & Baugh, C. M. 1995, MNRAS 273, L1

Goldenfeld, N. 1992, *Lectures on Phase Transitions and the Renormalization Group*, Addison Wesley (1992).

Goroff, M. H., Grinstein, B., Rey, S.-J., & Wise, M. B. 1986, ApJ, 311, 6

Gramann, M. 1992, ApJ, 401, 19

Hamilton, A. J. S., Kumar, P., Lu, E., & Matthews, A. 1991, ApJ , 374, L1

Jain, B. & Bertschinger, E. 1994, ApJ, 431, 495

Jain, B. & Bertschinger, E. 1995, preprint, astro-ph/9503025

Jain, B., Mo, H. J., & White, S. D. M. 1995, MNRAS, 276, L25

Jain, B. 1995, preprint, astro-ph/9509033

Juszkiewicz, R. 1981, MNRAS, 197, 931

Juszkiewicz, R., Bouchet, F. R., & Colombi, S. 1993, ApJ, 412, L9

Juszkiewicz, R., Sonoda, D. H., & Barrow, J. D. 1984, MNRAS, 209, 139

Lewin, L. 1981, *Polylogarithms and Associated Functions*, North Holland

Łokas, E. L., Juszkiewicz, R., Bouchet, F. R., & Hivon, E. 1995, preprint, astro-ph/9508032

Makino, N., Sasaki, M., & and Suto, Y. 1992, Phys. Rev. D, 46, 585

Nityananda, R. & Padmanabhan, T. 1994, MNRAS, 271, 976

Padmanabhan, T., Cen R., Ostriker J. P. & Summers F. J. 1995, preprint, astro-ph/9506051

Peacock, J. A. & Dodds, S. J. 1994, MNRAS, 267, 1020

Peebles, P. J. E. 1974, A&A, 32, 391

Peebles, P. J. E. 1980, *The Large-Scale Structure of the Universe*, Princeton University Press

Peebles, P. J. E. 1990, ApJ, 365, 27

Peebles, P. J. E. & Groth, E. J. 1976, A&A, 53, 131

Ryden, B. & Gramann, M. 1991, ApJ, 383, L33

Scoccimarro, R. & Frieman, J. 1996, ApJS, in press

Suto, Y., & Sasaki, M. 1991, Phys. Rev. Lett., 66, 264

Vishniac, E. T. 1983, MNRAS, 203, 345

Wise, M. B. 1988, in *The Early Universe*, W.G. Unruh and G. W. Semenoff (eds.), D. Reidel Publishing Company

Zel'dovich, Ya. B. 1965, Adv. Astron. Ap., 3, 241

This preprint was prepared with the AAS LaTeX macros v4.0.

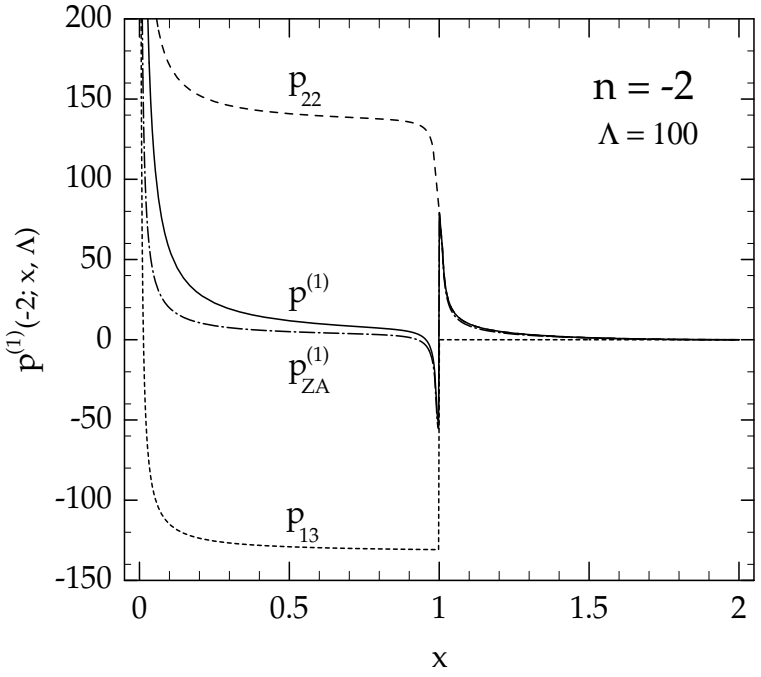

Fig. 6.— Same as Fig. 3 but for $n = -2$ and $\Lambda \equiv k_c/\epsilon = 100$. For reasons of clarity, we do not show the behavior for $x \leq 2\Lambda^{-1}$ ($k \leq 2\epsilon$), where p_{22} turns over to the scaling given in Eq. (3-7). Similarly, $p_{13} = 0$ when $x \leq \Lambda^{-1}$.

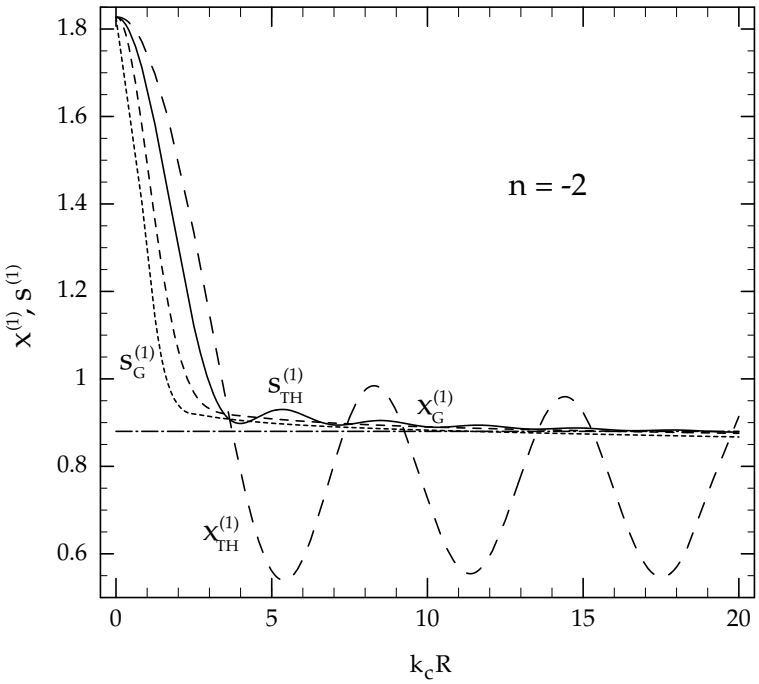

Fig. 7.— One-loop corrections to the average two-point correlation function $x^{(1)}$ and variance $s^{(1)}$ for $n = -2$ as a function of k_cR, for top-hat (TH) and Gaussian (G) smoothing. Solid curve shows $s^{(1)}_{\rm TH}$, dotted curve corresponds to $s^{(1)}_{\rm G}$, dashed curve shows $x^{(1)}_{\rm G}$, and the long-dashed curve $x^{(1)}_{\rm TH}$. The dot-dashed line shows the large-scale approximation given in Eqs. (3-39) and (3-41). For $k_cR = 0$ we recover the unsmoothed results $s^{(1)} = x^{(1)} \approx 1.82$ (Scoccimarro & Frieman 1996).

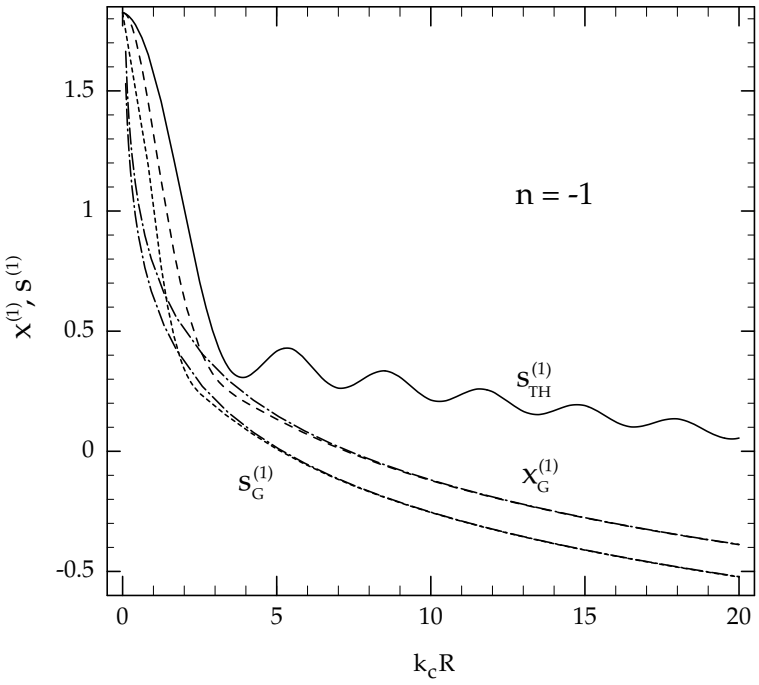

Fig. 8.— Same as Fig. 7 but for $n = -1$. Dot-dashed curves correspond to the large-scale approximation to the 1-loop coefficients, Eqs. (3-43) and (3-44). We do not show $x^{(1)}_{\rm TH}$, which undergoes large oscillations.

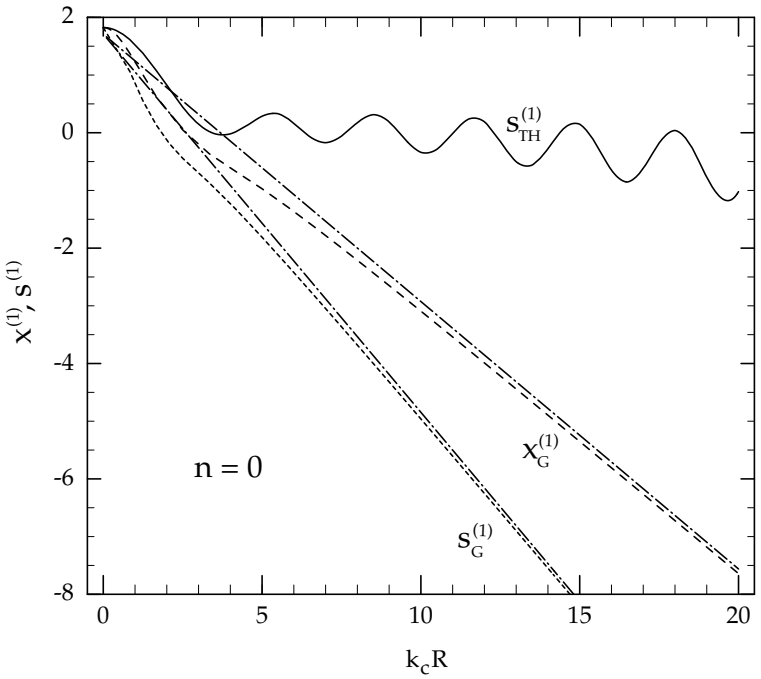

Fig. 9.— Same as Fig. 7 but for $n = 0$. Dot-dashed curves correspond to the large-scale approximation to the 1-loop coefficients, Eqs. (3-46) and (3-47).

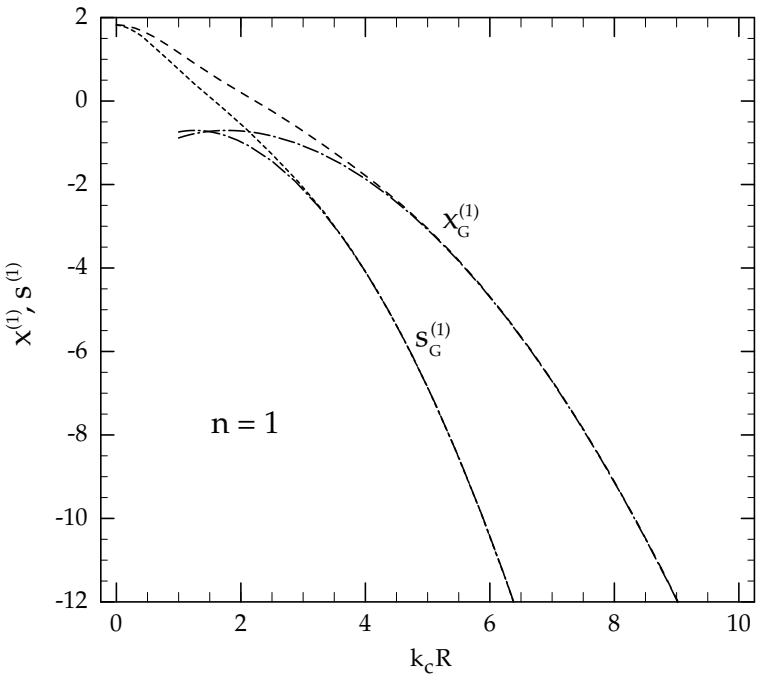

Fig. 10.— Same as Fig. 7 but for $n = 1$. Dot-dashed curves correspond to the large-scale approximation to 1-loop coefficients, Eqs. (3-49) and (3-50).

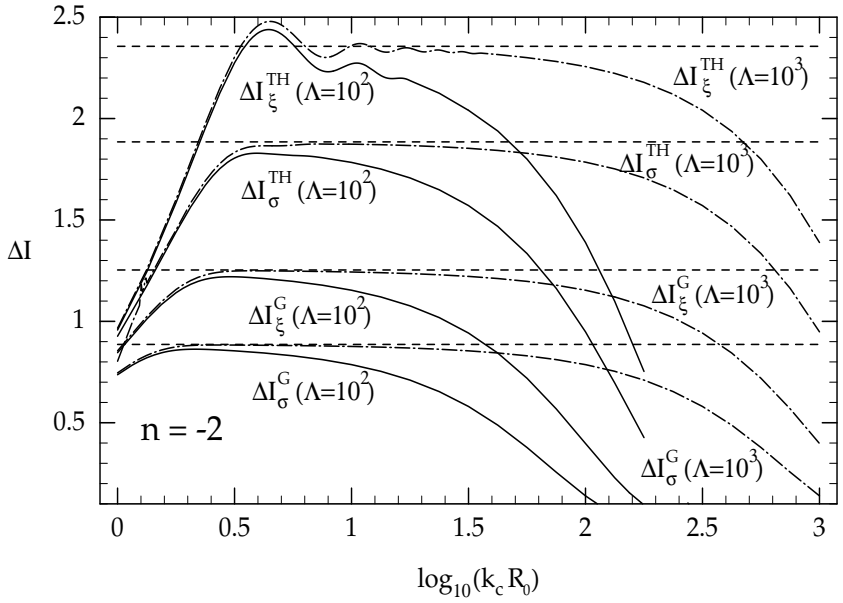

Fig. 11.— $\Delta I_{\sigma,\xi}(-2, k_c R_0, \Lambda)$ as a function of $k_c R_0$ for top-hat and Gaussian smoothing (see Eqs. (4-11) and (4-13) for definitions). Dashed lines represent the self-similar case (constant ΔI) in which the limit $\Lambda \equiv k_c/\epsilon \to \infty$ has been taken ($\epsilon \to 0$, $k_c \to \infty$). Dot-dashed curves denote the choice $\Lambda = 10^3$, solid curves correspond to $\Lambda = 10^2$. The differences between these curves and the $\Lambda \to \infty$ lines measure the deviations of the correlation length from self-similar evolution.

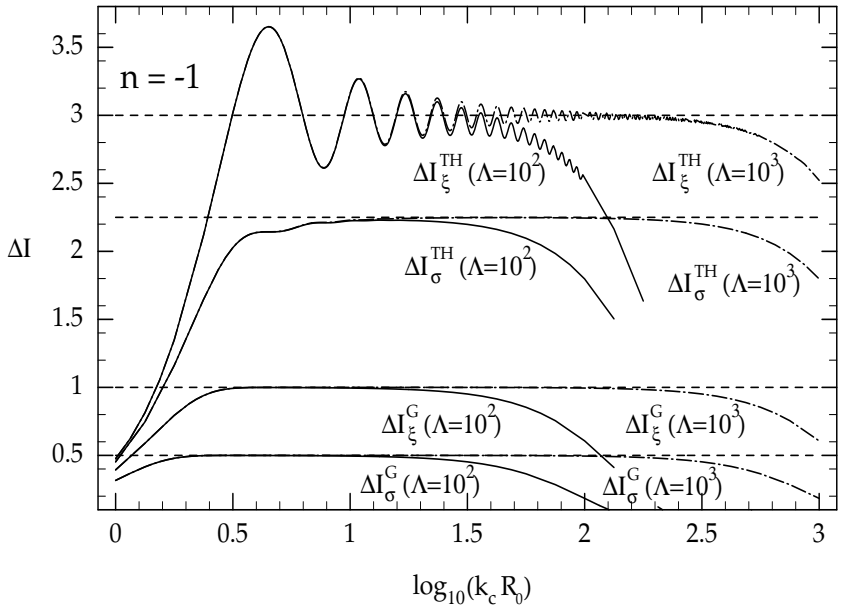

Fig. 12.— Same as Fig. 11 but for $n = -1$.

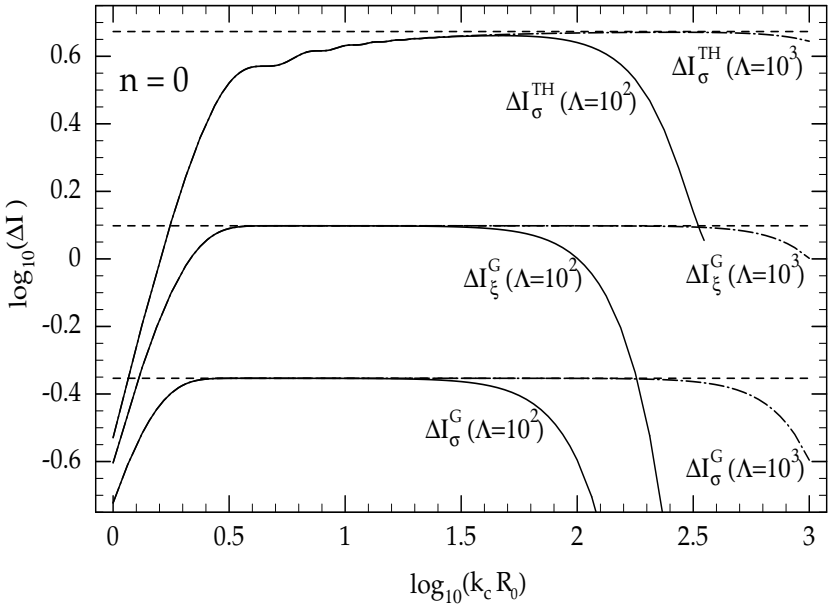

Fig. 13.— Same as Fig. 11 but for $n = 0$.

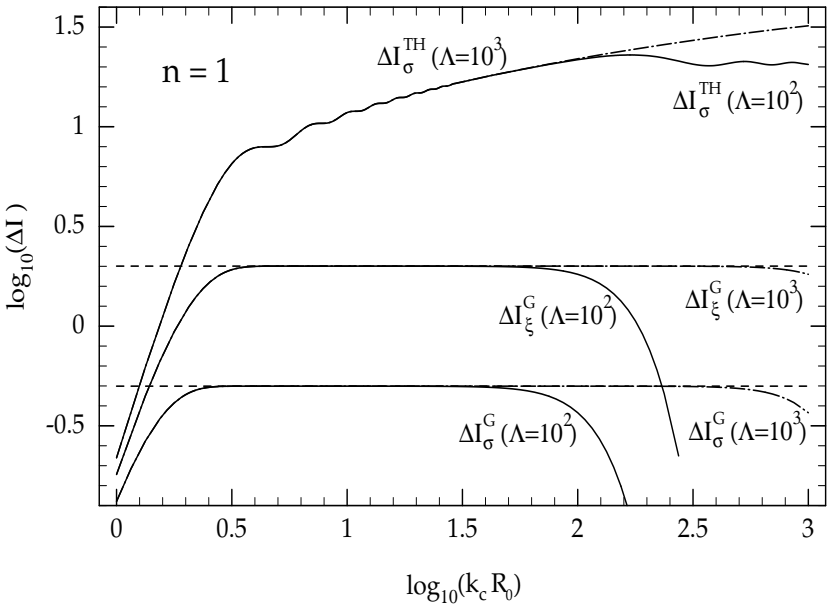

Fig. 14.— Same as Fig. 11 but for $n = 1$.

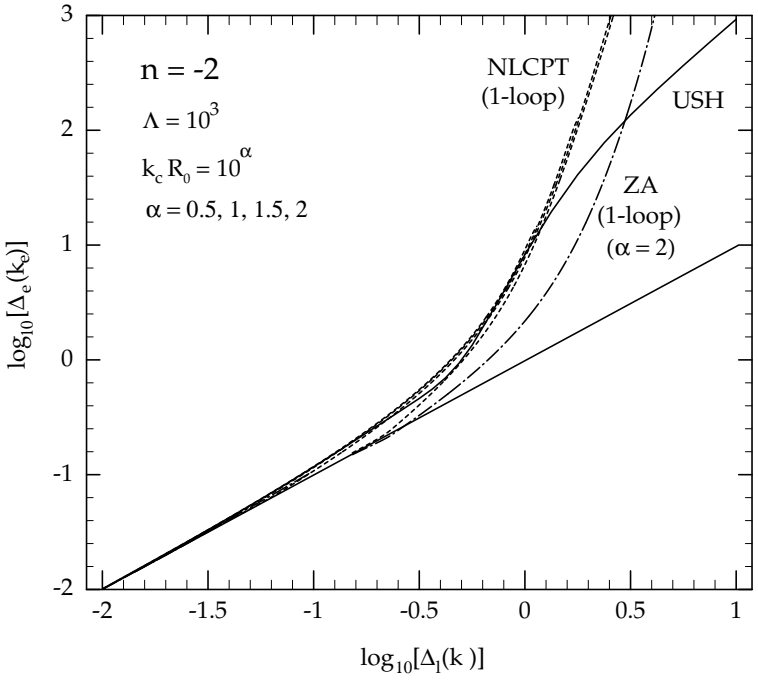

Fig. 15.— The evolved dimensionless power spectrum $\Delta_e(k_e)$ as a function of the linear dimensionless power spectrum $\Delta_\ell(k)$ for $n = -2$. The scales k_e and k are related according to Eq. (4-27). The solid curve shows the universal scaling hypothesis (USH); dotted curves correspond to the predictions of non-linear cosmological perturbation theory (NLCPT) including 1-loop corrections. The different NLCPT curves correspond to different values of $k_c R_0$ in the scaling region where self-similarity is expected to hold. The solid straight line corresponds to linear perturbation theory, whereas the dot-dashed curve is the prediction of the 1-loop Zel'dovich approximation for $k_c R_0 = 100$.

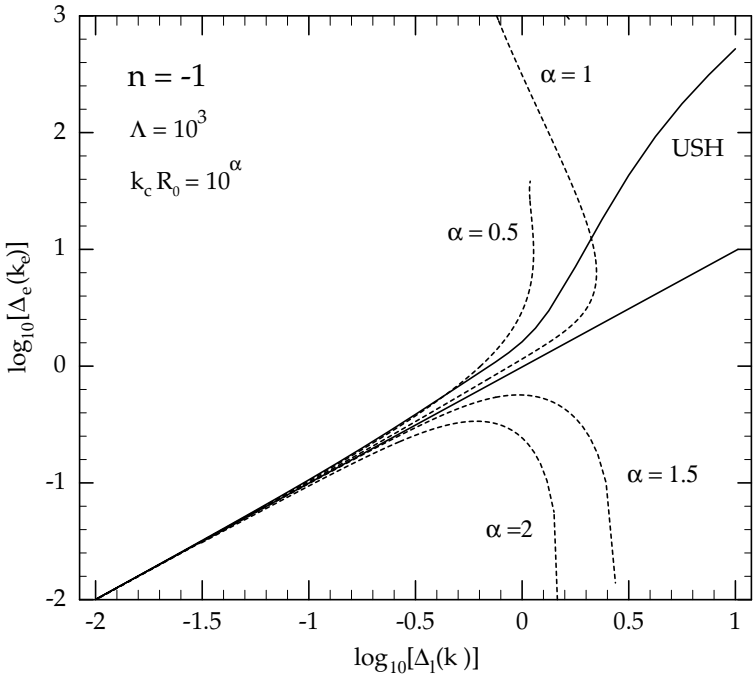

Fig. 16.— Same as Fig. 15 but for $n = -1$. Note the breaking of self-similarity.

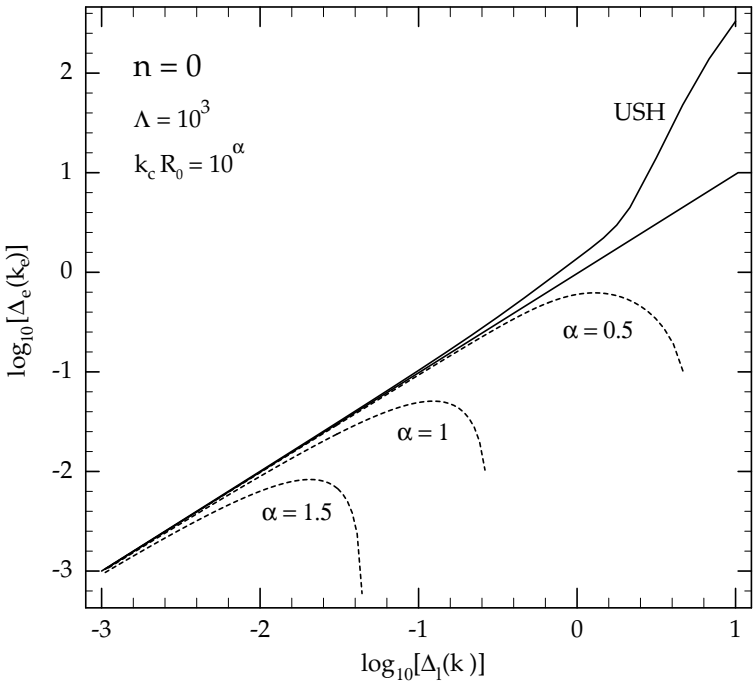

Fig. 17.— Same as Fig. 15 but for $n = 0$.

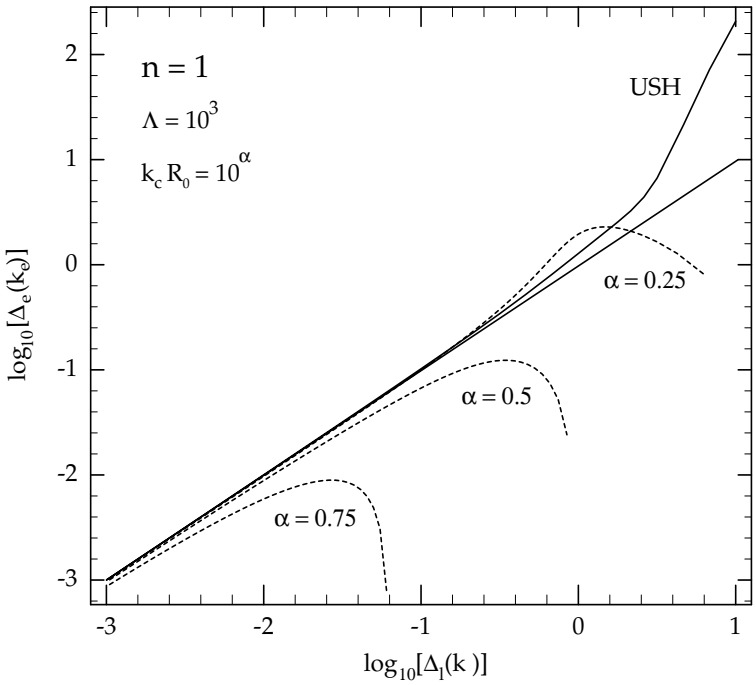

Fig. 18.— Same as Fig. 15 but for $n = 1$.

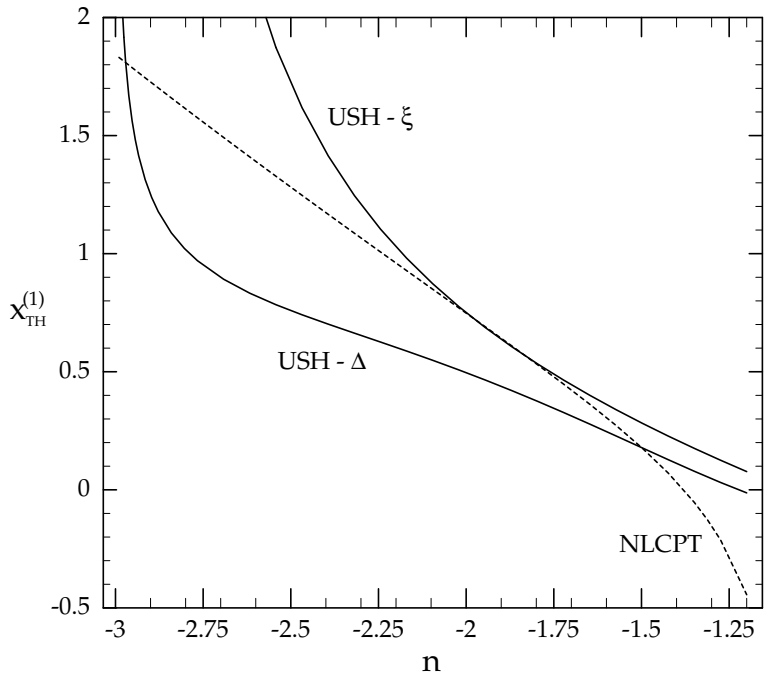

Fig. 19.— One-loop correction to the average correlation function, $x^{(1)}_{\rm TH}$, as a function of spectral index n in NLCPT (dotted curve) and in the USH obtained from the correlation function ansatz (solid curve labeled USH - ξ) and from the dimensionless power spectrum ansatz (USH - Δ).